# A Simple Ocean-Atmosphere Climate Model: Basic Model and a Simple Experiment[1]

PETER J. WEBSTER AND KA MING W. LAU

*Department of Atmospheric Sciences, University of Washington, Seattle 98195*

(Manuscript received 19 January 1977, in revised form 5 April 1977)

ABSTRACT

A simple model is developed with the aim of studying large-scale and long-term interactions between the various components of the earth-ocean-atmosphere system. The general three-dimensional structure of the system is simplified by division into a number of domains, so chosen as to isolate regions of similar character or similar lower boundary conditions. The governing primitive equations and boundary conditions are averaged in longitude between the limits of each domain and neighboring domains are allowed to interact via east-west interdomain fluxes of heat and momentum and lateral interdomain work terms, or, in the case of the adjacent oceanic and atmospheric domains, via vertical heat and momentum exchanges. From this processes, sets of two-dimensional coupled equations evolve in latitude-height space for both the atmosphere and the ocean.

Dynamic coupling of adjacent atmospheric domains is accomplished by the development of a new parameterization based on the theory of slowly varying or quasi-stationary modes. The character of the parameterization is such that it reduces to fluxes of quasi-geostrophic nature in middle and higher latitudes, whereas at low latitudes the fluxes are consistent with those associated with circulations confined to the longitude-height plane. Zonal fluxes of heat and momentum within each domain are handled by the baroclinic eddy parameterizations of Stone, Green and Wiin-Nielson and Sela.

Results are presented for the three-domain version of the domain-averaged model. The three domains, each of which extend from pole to pole, consist of an atmospheric domain surmounting a continental region and an atmospheric domain which lies over an interactive and dynamic ocean domain. The ocean is represented by a simple variable depth and temperature mixed layer model modified by a large-scale "thermohaline" circulation. Converged results for the dry model using equinoctial and Northern Hemisphere solsticial forcing are presented. Field magnitudes and distributions appear consistent with the implied boundary conditions. Differences between the two domains during the equinox are relatively small although surface temperatures over land are considerably warmer than over the ocean at low latitudes, whereas at high latitudes the reverse is apparent. At the solstice large variations occur in both hemispheres especially in the summer hemisphere, where a low-latitude easterly maximum occurs surmounting a weaker low-level westerly flow. In the subtropics near the region of maximum heating, the meridional flux of heat is from over land to over the ocean with heating rates of about 2 K day$^{-1}$, which is similar in magnitude to the poleward heat flux by the transient eddies in the winter hemisphere.

## 1. Introduction

In the search for an understanding of climate and climatic variability, meteorologists and oceanographers have long acknowledged the mutual importance of the interaction of oceans and atmosphere over a wide range of space and time scales. Smagorinsky (1953) showed, for example, that it was the dual role of continental and oceanic heating that was responsible for the structure of the mean seasonal climatology. On a much shorter time scale, Pyke (1965) explained the rapid development of cyclones in the proximity of the anomalous warm water regions near the eastern shores of continents. For periods beyond the synoptic, Shukla (1975) discussed the influence of the temperature of the Somali current on the behavior of the Indian summer monsoon; the reverse influence, that of local winds effecting the Somali circulation having been discussed by Leetma (1972). For still longer time scales Namias (1971, 1972, 1976) suggested that statistically significant correlations exist between large-scale sea-surface temperature anomalies and seasonal temperature and precipitation distributions over vast regions of the globe. Possible relationships between global atmospheric events and major El Niño's have been noted by Bjerknes (1969), Namias (1976), Ramage (1975) and many others. Trenberth (1976) extended the possible interaction range to at least that of the Southern Oscillation or beyond five or so years.

The small sampling of the many observational and

[1] Contribution No. 419, Department of Atmospheric Sciences, University of Washington.

theoretical studies indicates the real and important interactions that occur between atmospheric and oceanic systems. The problem arises, however, not in the appreciation that an interaction exists, but rather in how to elucidate the major physical mechanisms through which the interaction takes place. One method to approach such an elucidation is to study long series of detailed data of the atmosphere and ocean while another involves the development of and the experimentation with theoretical and numerical models. With a general lack of detailed observations and, in a climatic sense, relatively short data series, an increasing emphasis has been placed on the building of large-scale ocean-atmosphere models.

A variety of model species have been utilized in an attempt to simulate climatic structure and variability. These different types range from the energy balance models (e.g., Budyko, 1969; Sellers, 1969; Schneider and Gal-Chen, 1973; North, 1975a,b; and many others) to the complicated and sophisticated general circulation models (e.g., Manabe *et al.*, 1965; Arakawa *et al.*, 1968; Washington and Kasahara, 1970; Holloway and Manabe, 1971; and many others). Both possess inherent attributes and drawbacks. The simplicity and ease of computation of the energy balance models are clearly advantages but this simplicity is equally a disadvantage as only a few of the many potentially important feedback mechanisms are included in the model formulation. Conversely, the sophistication of the large general circulation models allows for the possibility of the inclusion of most important physical processes, but this detail itself renders experimentation difficult and expensive. Experimentation is usually accomplished by comparison of statistics generated from a "standard" or "control" run with statistics generated with the modified run (e.g., Manabe and Terpstra, 1974). Such experiments can suggest relative roles of various factors although often the amount of material produced renders analysis a difficult problem.

Beyond these difficulties, the general circulation models possess substantial simulation skill which can be analyzed (e.g., Hayashi, 1974), although such analysis requires tools at least as sophisticated as those required for real data analysis. Furthermore, the models are capable of lending valuable insights into complicated processes. For example, the coupled ocean-atmosphere models of Bryan *et al.* (1975) and Manabe *et al.* (1975) have succeeded in underlining the importance in the treatment of the total system as a necessary prerequisite in providing an adequate description of even the mean climatic state. However, based on the premise that a large ratio is required between the length of the numerical experiment and the time scale of the interactions between the components of the total system, the resources required for extended runs for periods of years, given current technology, suggest an impracticality, not because of any inadequacy of the large models, but merely from a logistical point of view.

At the other end of the spectrum, the use of energy balance models for the study of climatic processes of the scale of years is most probably unsuitable—principally because of the simple representation of the dynamics, which are at best relegated to a diffusive role (North, 1975b) or neglected altogether.

The gap left between the energy balance and general circulation models has led to the development of a third class of models—those which are either simplified general circulation models or which are phenomenological in nature, with specific emphasis on one or a few hopefully important physical interactions rather than attempting a detailed simulation of the system. The simplification of the general circulation models is normally achieved by neglecting the zonal dimensions, resulting in the zonally symmetric model (e.g., Hunt, 1973; McCracken, 1974) or the zonally averaged model where the eddy flux quantities are parameterized by the use of some closure assumption (e.g., Wiin-Nielson and Sela, 1971). Such models possess the desirable aspect of being sufficiently simple to allow extended integration. However, more rapid integration time must be balanced against the neglect of longitudinal differences and the simplification of the role of baroclinic eddies.

The first zonally averaged model to include an ocean was developed by Pike (1971) to study the mutual dependence of low-latitude atmospheric and oceanic circulations. Whereas Pike's model serves well the reason for its development, it is inappropriate for the study of climate even though it introduces into the atmosphere oceanic time scales via interactive processes. The principal reason for the inappropriateness is that, like all zonally averaged models, it does not allow for the thermal contrast between land and ocean in the meridional direction—a thermal contrast which changes polarity as a function of season and which allows for the interaction of different thermal lags (i.e., land and ocean) which are responsible for a large component of the annual cycle.

The preceding discussion suggests the following attributes which a model should possess in order to study climatic variations associated with ocean-atmosphere interactions:

1. The model should be sufficiently sophisticated to represent the basic structure of the atmosphere and the ocean and be able to account for their interaction.
2. The model should be sufficiently simple and efficient to allow for extended integration for periods well beyond the time-scales of the ocean-atmosphere interaction.
3. The model should include both the land and ocean region (i.e., the oceans should be finite in lateral extent) and each region should be modeled explicitly.

In this paper we will attempt to develop a model which contains the essence of some of the desirable

properties described above. Such a development follows a structure suggested by Lahiff (1975). Lahiff divided a zonally symmetric model into a series of latitudinal domains and averaged the system in both latitude and height for each domain. The result was a system of coupled algebraic equations with which Lahiff was able to simulate some aspects of the atmospheric climate. We deviate from Lahiff by allowing our domains to have a *longitudinal* extent which is only averaged in the zonal sense and *then only to the limits of each domain.* We deviate further by applying no averaging in the vertical or latitudinal directions. The domains are defined so as to include regions of similar character (e.g., the atmosphere and the ocean) and regions of similar lower boundary conditions (e.g., the atmosphere over the continents and the atmosphere over the ocean) as shown in the example in Fig. 2. What emerges are systems of differential equations (as distinct from Lahiff's algebraic set) which are functions of *time, height* and *latitude* for *each* domain. Interaction between the domains in the form of heat and momentum fluxes and the work each domain does on its neighbor appear as quantities which need evaluation at the boundaries of the domains. This evaluation requires the development of a new parameterization.

We offer here, then, one further model of that third class—the phenomenological group—which will hopefully alleviate some of the problems associated with other model types and also of other phenomenological models. In particular, it is designed to run efficiently and cheaply so that runs of the order of years are conceivable. Further, it contains an explicit representation of land and ocean differences allowing for an approach toward the difficult partition between standing and transient eddy effects. The ocean model to which the atmosphere is coupled is a very simple two-layer dynamic model capable of advecting heat.

It should be emphasized that the domain-averaged model was not developed with the idea of attempting those tasks which the other models do so well. For example, it does not try to approach a careful and detailed simulation of the atmospheric mean structure as do the large-scale general circulation models. Nor does it aim at integrations extending over centuries nor seek the sensitivity of the atmosphere to subtle variations in external climatic controls as attempted by the energy balance models. Rather the model has been developed with one time scale and one class of phenomena in mind, *viz.*, the interactions between various components of the earth-atmosphere-ocean system with time scales extending from monsoonal to interannual.

In the next section the theoretical framework of the domain-averaged model is developed along with the basic equations of the atmosphere and ocean parts. In Section 3 the problem is closed by the development of a system of parameterizations representing the poleward transports of heat and momentum by the transient eddies and also the east-west fluxes of heat and momentum and interaction terms. Section 4 discusses the various heating and dissipation laws. A prototype of the model is specialized into a system of two-layer models in Section 5 and converged fields for the equinox and solstice cases are presented. The model is critically discussed in Section 6.

## 2. The basic model

### a. The atmosphere

The primitive equations of motion in spherical coordinates may be written in the flux form

$$\left.\begin{aligned} u_t+g(u)&=-\frac{1}{a\cos\phi}\psi_\lambda+v\left(f+\frac{\tan\phi}{a}u\right)+F_1\\ v_t+g(v)&=-\frac{1}{a}\psi_\phi-u\left(f+\frac{\tan\phi}{a}u\right)+F_2\\ T_t+g(T)&=\mathrm{K}\omega T/p+\dot{Q}+F_3\\ q_t+g(q)&=S+F_4\\ \psi_p&=-RT/p\\ \omega_p+\frac{1}{a\cos\phi}(v\cos\phi)_\phi+\frac{1}{a\cos\phi}u_\lambda&=0 \end{aligned}\right\}, \quad (1)$$

where

$$g(X)=\frac{1}{a\cos\phi}(Xu)_\lambda+\frac{1}{a\cos\phi}(Xv\cos\phi)_\phi+(X\omega)_p.$$

In Eq. (1), $\lambda$, $\phi$ and $p$ represent the three independent variables of longitude, latitude and pressure, respectively, and $F_i$ represents vertical and subgrid-scale processes, $\dot{Q}$ the nonadiabatic heating effects and $S$ the source and sink of moisture.

We now divide longitude into a total of $K$ domains which have common boundaries at the meridians $\lambda_1, \lambda_2, \ldots, \lambda_K, \lambda_1$ as indicated in Fig. 1. Further, we define $\bar{X}_k$ as the mean value of some quantity $X$ in the $k$th domain and $X'_k$ as the deviation from $\bar{X}_k$. Such a breakdown of the longitude structure of variable $X$ suggests the following integral relationships:

$$\left.\begin{aligned} X_k(\lambda,\phi,p,t)&=\bar{X}_k(\phi,p,t)+X'_k(\lambda,\phi,p,t)\\ \int_{\lambda_{k-1}}^{\lambda_k}X_k\partial\lambda&=\bar{X}_k(\lambda_k-\lambda_{k-1})\\ \int_{\lambda_{k-1}}^{\lambda_k}X_k'\partial\lambda&=0\\ \int_{\lambda_{k-1}}^{\lambda_k}\frac{\partial X}{\partial\lambda}\partial\lambda&=X(\lambda_k)-X(\lambda_{k-1}) \end{aligned}\right\}. \quad (2)$$

In terms of the notation adopted in (2), we can define the total zonal average of quantity $X$ as

$$\langle X\rangle=\frac{1}{2\pi}\sum_{k=1,K}(\lambda_k-\lambda_{k-1})\bar{X}_k. \tag{3}$$

The relationships shown in Eqs. (2) and (3) illustrate the concept of domain averaging in longitude. If $K=1$ the problem reduces to the conventional zonally averaged model (e.g., Hunt, 1973 and McCracken, 1973) with $X(\lambda_k)=X(\lambda_{k-1})$. In that special case the zonal derivatives vanish. In the general case of $K$ domains, such derivatives reduce to the differences of the perturbation quantities evaluated at the longitudinal boundaries of each domain. Even though the individual deviations summed in longitude between 0 and $2\pi$ must vanish, a point which will later allow an integral constraint on the calculation of the deviations, each derivative provides information regarding the interaction of each domain with its neighbors. Such terms act as physical links between adjacent domains.

With the integral relationships defined in (2), the basic equation set (1) may be rewritten to represent the basic state of the $k$th domain. The basic set becomes

$$\left.\begin{aligned}
&\bar{u}_t=f\bar{v}-\bar{M}(\bar{u})+\bar{D}(u')+\bar{I}(\lambda)+\bar{F}_1\\
&\bar{v}_t=-f\bar{u}-\bar{M}(\bar{v})+\bar{D}(v')+\bar{I}(\phi)+\bar{F}_2+(1/a)\bar{\psi}_\phi\\
&\bar{T}_t=-\bar{M}(\bar{T})+\bar{D}(T')+\bar{I}(T)+\bar{F}_3+\bar{Q}\\
&\bar{q}_t=-\bar{M}(\bar{q})+\bar{D}(q')+\bar{I}(q)+\bar{F}_4+S\\
&\bar{\omega}_p+(1/a\cos\phi)(\bar{v}\cos\phi)_\phi=\bar{I}(m)\\
&\bar{\psi}_p=-R\bar{T}/p
\end{aligned}\right\}. \tag{4}$$

The subscript denoting the $k$th domain introduced in (2) will be subsequently assumed.

In the above set $\bar{M}(\bar{X})$ represents the meridional and vertical flux convergence of $\bar{X}$ by the mean motions of the $k$th domain, which are defined by

$$\left.\begin{aligned}
\bar{M}(\bar{u})&=\frac{1}{a\cos\phi}(\bar{u}\bar{v}\cos\phi)_\phi+(\bar{u}\bar{\omega})_p-\frac{1}{a}\bar{u}\bar{v}\tan\phi\\
\bar{M}(\bar{v})&=\frac{1}{a\cos\phi}(\bar{v}\bar{v}\cos\phi)_\phi+(\bar{v}\bar{\omega})_p+\frac{1}{a}\bar{u}\bar{u}\tan\phi\\
\bar{M}(\bar{T})&=\frac{1}{a\cos\phi}(\bar{T}\bar{v}\cos\phi)_\phi+(\bar{T}\bar{\omega})_p-\frac{K\bar{\omega}\bar{T}}{p}\\
\bar{M}(\bar{q})&=\frac{1}{a\cos\phi}(\bar{q}\bar{v}\cos\phi)_\phi+(\bar{q}\bar{\omega})_p
\end{aligned}\right\}. \tag{5}$$

Here $\bar{D}(X')$ represent the meridional and vertical flux convergences by deviations from the averages in the $k$th domain. These may be written as

$$\left.\begin{aligned}
\bar{D}(u')&=-\frac{1}{a\cos\phi}(\overline{u'v'}\cos\phi)_\phi-(\overline{u'\omega'})_p+\frac{1}{a}\overline{u'v'}\tan\phi\\
\bar{D}(v')&=-\frac{1}{a\cos\phi}(\overline{v'v'}\cos\phi)_\phi-(\overline{v'\omega'})_p-\frac{1}{a}\overline{u'u'}\tan\phi\\
\bar{D}(T')&=-\frac{1}{a\cos\phi}(\overline{T'v'}\cos\phi)_\phi-(T'\omega')_p+\frac{K}{p}\overline{\omega'T'}\\
\bar{D}(q')&=-\frac{1}{a\cos\phi}(\overline{q'v'}\cos\phi)_\phi-(\overline{q'\omega'})_p
\end{aligned}\right\}. \tag{6}$$

The zonal fluxes and interdomain interaction terms are represented by $\bar{I}$ which are defined by

$$\left.\begin{aligned}
\bar{I}(\lambda)&=-\frac{1}{a\cos\phi}[u(\lambda_k)^2-u(\lambda_{k-1})^2]d_k\\
&\quad-\frac{1}{a\cos\phi}[\psi(\lambda_k)-\psi(\lambda_{k-1})]d_k\\
\bar{I}(\phi)&=-\frac{1}{a\cos\phi}[u(\lambda_k)v(\lambda_k)-u(\lambda_{k-1})v(\lambda_{k-1})]d_k\\
\bar{I}(T)&=-\frac{1}{a\cos\phi}[u(\lambda_k)T(\lambda_k)-u(\lambda_{k-1})T(\lambda_{k-1})]d_k\\
\bar{I}(q)&=-\frac{1}{a\cos\phi}[u(\lambda_k)q(\lambda_k)-u(\lambda_{k-1})q(\lambda_{k-1})]d_k\\
\bar{I}(m)&=-\frac{1}{a\cos\phi}[u(\lambda_k)-u(\lambda_{k-1})]d_k
\end{aligned}\right\}. \tag{7}$$

where $d_k=(\lambda_k-\lambda_{k-1})^{-1}$.

Equation set (4), together with the definitions (5)–(7), represents the mean structure of the $k$th longitudinal domain of a domain-averaged model. Written in this manner, a set of $K$ systems of equations emerges in $(\phi,p,t)$ space. Closure of the systems depends upon the determination of the meridional and vertical flux convergence $\bar{D}(X')$ and the interdomain or zonal fluxes $\bar{I}$ as functions of the mean variables of each domain. It should be noted that the interdomain terms shown in (7) have been expressed as differences of terms evaluated at points in space. Consequently, not only need we relate deviation covariances to functions of the mean variables, which is the usual problem encountered in zonally averaged models, but we also need to relate the mean structure of each domain to variables evaluated at *points* within that domain.

Besides the determination of the $\bar{D}$ and $\bar{I}$ functions, we also require expressions for $\bar{F}_i$, $\bar{Q}$ and $\bar{S}$ for each domain. If the zonal extent of each domain is so chosen as to correspond to a lower boundary of similar or uniform character (e.g., an atmospheric domain may

be chosen to extend over a continental region whereas the neighboring atmospheric domain may lie over a domain-averaged ocean) then $\bar{F}_i$, $\bar{Q}$ and $\bar{S}$ may be defined simply and unambiguously for each domain. Consequently, the mean structure of each domain will depend upon different sets of parameters, but, at the same time, will be functions of the mean state of all neighboring domains through the zonal fluxes and interaction terms $\bar{I}$.

As the main aim of this paper is to develop the concept of the domain-averaged model with emphasis on the atmospheric part of the model, we will utilize its simplest prototype. Such a model consists of two atmospheric domains of equal longitudinal extent. One atmosphere resides over a pole-to-pole continental region, while the second extends over the most simple interactive and dynamic ocean. Such a system is shown in Fig. 2. Details of the ocean domain structure are discussed below.

### *b. The ocean*

The development of an ocean model which was compatible with the simple atmosphere presented a considerable challenge. The first choice was the relatively simple one-dimensional energy balance model developed by Kraus and Turner (1967) and Turner and Kraus (1967), hereafter refered to as the KT model. The model was chosen because it provides a simple interaction between the atmosphere and the ocean, and because of its general representativeness of much of the observed character of at least the sea-surface temperature at mid-latitude providing relatively accurate lag times between solar heating and sea-surface temperature maxima.

Unfortunately, the extention of the KT model to a global domain, in which the surface temperature and mixed-layer depth were calculated at each latitude grid point, appeared to extend the model beyond the physical limitations within which it was defined. For example, at very low latitudes, in regions of strong insolation and relatively weak wind stress, the KT model predicted an ever deepening and warming mixed layer. Apparent in these results was that a one-dimensional energy balance model could not adequately describe the equatorial ocean where lateral heat transports may be of considerable importance. To overcome the shortcomings of KT

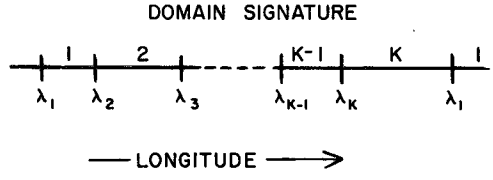


FIG. 1. Schematic representation of the domain signature of a domain-averaged model. The $k$th domain is bordered by the meridians $\lambda_k$ and $\lambda_{k-1}$.

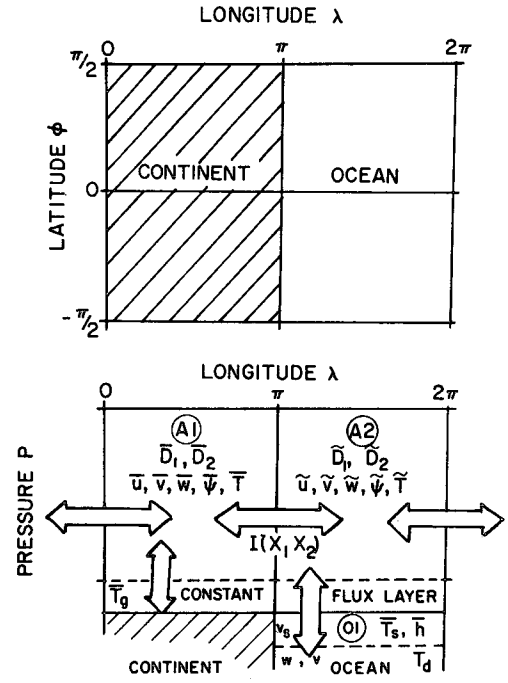


FIG. 2. Latitude-longitude (upper diagram) and latitude-pressure sections (lower diagram) of a two atmosphere and one ocean domain-averaged model. One atmosphere A1 surmounts the continental region, whereas A2 lies over the interactive advective mixed layer ocean O1. Variables defining the mean structure of each domain are indicated. Interdomain fluxes and interaction terms are indicated by $I$.

model, advection and a more appropriate dissipation mechanism were included. The modified KT model (hereafter referred to as the AKT model) is discussed in detail by Lau (1976). In this paper we will present only the basic structure and some general properties.

The AKT model is schematically described in Fig. 3. The upper part of the ocean consists of a well-mixed layer of variable depth $\bar{h}$ of temperature $\bar{T}_s$. The lower part of the ocean is separated from the upper by an abrupt density change which is represented by a heavy dashed line. The large-scale circulation in the upper and lower layers and between the layers is represented by heavy arrows. The heat and mechanical energy inputs are shown on the surface of the ocean. Stippling indicates regions where there exists no density discontinuity between the mixed layer and the lower ocean. In such regions convective adjustment modifies the oceanic column during cooling. The ice regime is indicated near the North and South Poles. Both the ice regions and the convective adjustment regions will be seen to vary with latitude as strong functions of time.

The governing equations for the temperature $\bar{T}_s$ of the mixed layer, the depth $\bar{h}$ of the mixed layer and the temperature $\bar{T}_{-h}$ of the ocean just below the thermocline are given by

$$(\bar{T}_s)_t + \bar{\mathbf{V}}_s \cdot \nabla \bar{T}_s + \Gamma \bar{w}_{-h} = (2/\bar{h}^2)[-(G^* - D^* - \bar{w}^*_{-h} K^*) + \bar{J}(-\bar{h})], \quad (8)$$

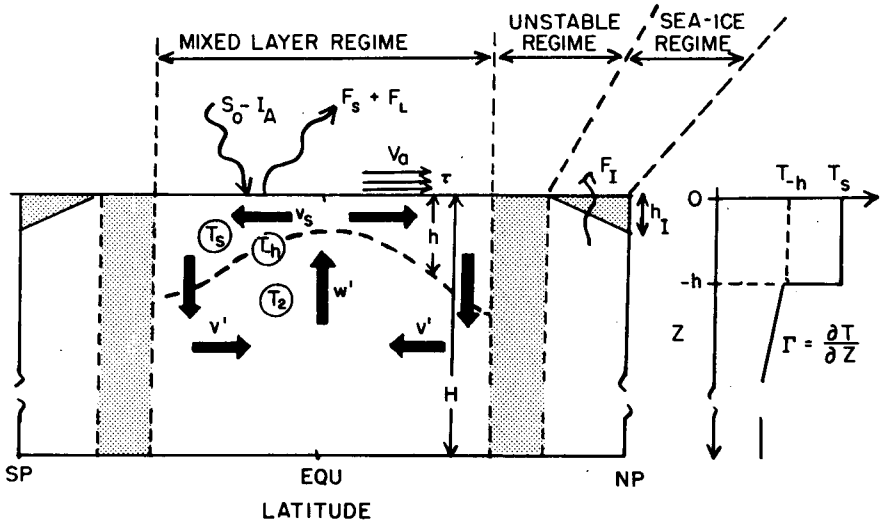


FIG. 3. Detailed schematic depth-latitude section of the advective mixed-layer ocean model. The mixed-layer regime, the unstable regime and the sea-ice regime are indicated by dashed lines and the simple meridional circulation by solid arrows. The mixed layer is defined to lie above the heavy dashed lines. The surface heat balance and wind stress terms are defined in the text. The corresponding vertical temperature structure is shown on the right.

$$\Delta(\bar{h}_t+\bar{\mathbf{V}}_s\cdot\nabla\bar{h}+\bar{w}_{-h}) = 2[(G^*-D^*)+\bar{h}I(-\bar{h})-2\bar{J}(-\bar{h})] \times[\bar{h}(\bar{T}_s-\bar{T}_{-h})+2K^*]^{-1}, \quad (9)$$

$$(\bar{T}_{-h})_t+\bar{w}^*_{-h}\Gamma=R_z(-h), \quad (10)$$

where

$$\bar{w}^*_{-h}=\bar{h}_t+\bar{\mathbf{V}}_s\cdot\nabla\bar{h}+\bar{w}_{-h},$$

$\bar{\mathbf{V}}_s$ is the large-scale horizontal velocity vector, $\Gamma$ the temperature lapse rate below the mixed layer, $\bar{\mathbf{V}}_s$ the horizontal velocity vector of the large-scale thermohaline circulation and $\bar{w}_{-h}$ the associated large-scale vertical velocity component evaluated at $z=-h$; $\bar{w}^*_{-h}$ represents the total vertical velocity through the interface at $z=-h$ and is a combination of $\bar{w}_{-h}$ and wind-induced eddy motion at the interface. $\Delta$ is the Heaviside function which modifies the structure of (9) such that if $\bar{w}^*_{-h}\leqslant 0$ (i.e., no entrainment of cold lower water), $\Delta=0$, but if $\bar{w}^*_{-h}>0$ (i.e., entrainment) then $\Delta=1$. We assume $\Gamma$ to possess the constant value of 0.003 K m$^{-1}$.

$G^*$ and $D^*$ represent the energy input by the wind stress $\tau$ and the dissipation within the mixed layer; $K^*$ represents the kinetic energy in the mixed layer $(\alpha\bar{\mathbf{V}}_s^2)$; $R$ is the incident solar radiation; $\bar{I}(z)$ the net energy gain by the layer given by

$$\bar{I}(z)=R(0)-R(-z)-F^*,$$

where $F^*$ is the total upward flux of latent and sensible heat; and $\bar{I}(z)$ is the integral of $I(z)$ between $-z$ and 0. $R(z)$ has been assumed to have an $e$-folding absorption of 10 m.

The derivation of (8) and (10) follows closely that of Kraus and Turner (1967) and Denman (1973). Denman modified the KT model by adding a climatologically determined $\bar{w}_{-h}$. If $\bar{V}$ and $\bar{w}_{-h}$ are set equal to zero and $\bar{T}_{-h}$ treated as constant, the KT model emerges from (8)–(10).

Closure of the ocean model requires expressions for the horizontal and vertical velocity components $\bar{\mathbf{V}}_s$ and $\bar{w}^*_{-h}$. It is assumed that the large-scale circulation is a result of the density differences existing in the ocean between middle and higher latitudes. To quantify this Lau calculates the vertically integrated pressure gradient force acting on the lower layer of the ocean model, which is given by

$$-\frac{1}{a\bar{\rho}_2}\bar{p}_\phi=-\frac{1}{\bar{\rho}_2 a}\left[\int_0^{H-h}\bar{\rho}g\,dz\right]_\phi \approx-\frac{gH}{\bar{\rho}_2 a}[(\bar{\rho}_1-\bar{\rho}_2)\bar{h}_\phi-\bar{h}(\bar{\rho}_1-\bar{\rho}_2)_\phi],$$

where it is assumed that $H\gg\bar{h}$ and $\bar{\rho}_i=\rho_0(1-\alpha\bar{T}_i)$, where $i=1, 2$ and $\rho_0$ is the density of water at 0°C. Subscripts 1 and 2 refer to quantities just above and just below the density interface. Here we have neglected salinity effects. A thermal driving force per unit mass is then given by

$$-\frac{1}{\bar{\rho}_2 Ha}\bar{p}_\phi=(\bar{T}_1-\bar{T}_2)\frac{\alpha g}{a}\bar{h}_\phi+\frac{g\bar{h}\alpha}{a}(\bar{T}_1-\bar{T}_2)_\phi, \quad (11)$$

which drives a perturbation meridional current in the lower layer, i.e.,

$$\bar{v}'=A[(\alpha g/a)(\bar{T}_s-\bar{T}_2)\bar{h}_\phi+(gh\alpha/a)(\bar{T}_s-\bar{T}_2)_\phi], \quad (12)$$

where $\bar{T}_1=\bar{T}_s$. Eq. (12) forms the basis for the parameterization of the meridional current of the ocean circulation. Applying the continuity equation to the lower layer gives the large-scale vertical velocity

$$\bar{w}_{-h}=-(H/a\cos\phi)(\bar{v}'\cos\phi)_\phi. \tag{13}$$

Furthermore, if we assume that the vertically integrated velocity is nondivergent, we can solve for the mixed-layer velocity field, *viz.*,

$$\bar{v}_s\rho_s\bar{h}+\bar{v}'\bar{\rho}_2(H-\bar{h})=0. \tag{14}$$

Eqs. (12), (13) and (14) thus parameterize the large-scale motion field in terms of the variables $\bar{T}_s$, $\bar{T}_{-h}$ and $\bar{w}_{-h}$. Eqs. (8)–(10) and (12)–(14) form a closed set given the heat balance at the surface and the atmospheric wind stress. In (12) $A$ is a free time-scale parameter, chosen as $5\times10^4$ s to produce large-scale upwelling of 1–5 cm day$^{-1}$, in keeping with the observations of Wyrtki (1961) for the open ocean. We further assume that integrated over all latitudes $\bar{w}_{-h}$ is zero.

Dissipation through the entire mixed layer enters the system via $D^*$ in (8) and (9). The formulation we use is identical to that of Alexander and Kim (1976). If we define the energy input by the wind as

$$G^*=(\eta_G/\rho_0\alpha g^2)(\tau/\rho_0)^{\frac{3}{2}},$$

where $\eta_G$ is a dimensionless constant and $\tau$ the wind stress at the surface of the ocean, then the net work done on the layer by the wind stress (i.e., energy input less dissipation) is given by

$$G^*-D^*=\{\eta_G-\eta_D[1-\exp(-\gamma h)]-\epsilon_m h/(\tau/\rho_0)^{\frac{3}{2}}\}\times(\tau/\rho_0)^{\frac{3}{2}}(\rho_0\alpha g^2)^{-1}. \tag{15}$$

Here $\epsilon_m$ is the background dissipation, $\eta_D$ a dimensionless constant and $\gamma$ the penetration depth of the dissipation. We use the values $\epsilon_M=2\times10^{-8}$ m$^2$ s$^{-3}$ and $\gamma=0.05$ m$^{-1}$ from Alexander and Kim (1976) and set $\eta_G=\eta_D=1.75$ from Kato and Phillips (1969).

Examination of (9) suggests a singularity when $\bar{T}_s=\bar{T}_{-h}+2K^*$. This happens when the column becomes convectively unstable and occurs at high latitudes equatorward of the ice limit. To account for this a convective adjustment is made to mix the cool surface water through the column. The convective adjustment process is schematically shown in Fig. 4. When the column temperature falls to 271 K ice is allowed to form and an analytic ice thickness distribution is assumed between the formation point and the pole. The temperature of the upper surface of the ice is calculated from heat balance considerations which will be discussed in Section 4. Melting of the ice occurs when the surface temperature rises above 273 K with the amount of melting being proportional to the heating excess.

Comparisons between the surface temperature and mixed-layer thicknesses of the AKT and KT models are shown in Fig. 5. The effects of the inclusion of

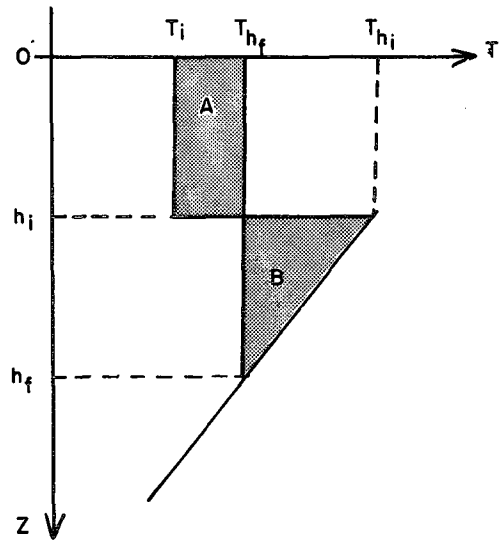


FIG. 4. Schematic representation of convective adjustment process if mixed layer becomes unstable (i.e., $\bar{T}_s\leqslant\bar{T}_{-h}$). Initial mixed-layer state ($\bar{T}_s=\bar{T}_i$, $\bar{h}=\bar{h}_i$) is mixed to stable state ($\bar{T}f$,$\bar{h}f$). Mixing is constrained so that area A is equal to area B.

advection can be seen immediately. First, $\bar{h}$ and $\bar{T}_s$ remain constant after the first year at low latitudes, whereas the one-dimensional KT model shows progressive deepening and warming of the mixed layer. Second, the high-latitude oceans are somewhat warmer with the inclusion of advection. Further, Lau shows that the amount of heat transported by the simple advective processes is substantial, representing about 30–40% of the observed atmospheric poleward transports which is similar to the residual estimates of Palmén and Newton (1969).

In summary, it appears that the AKT model is a compatible and interactive adjunct of domain-averaged atmosphere, providing not only heat fluxes, which bear strong similarity in both magnitude and location to observations (Lau, 1976), but also an annual cycle of $\bar{h}$ and $\bar{T}_s$ which is reproducible in time for the same boundary condition variation, at least after the first year.

## 3. Eddy flux parameterizations

Studies of atmospheric data suggest that the transportation of heat and momentum is accomplished by the actions of the zonally averaged motions and eddy motions. A major aim of the domain-averaged formulation was to model a similar partition of transportation roles. The following paragraphs detail a *first* attempt to model the mean and eddy flux transportations. A critical appraisal of the formulation and the need for a unified parameterization will be given in Section 6.

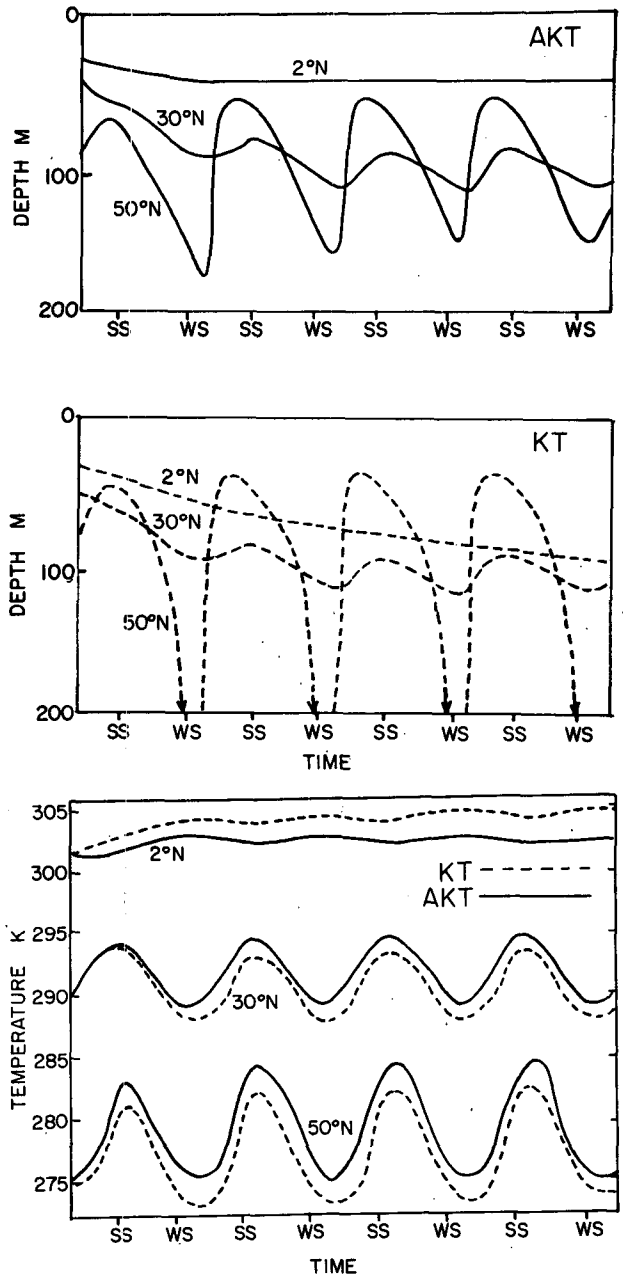


FIG. 5. Seasonal variation of (a) the mixed-layer depth ($\bar{h}$) at 2°, 30° and 50°N as simulated by the Kraus-Turner mixed-layer model (KT, dashed curves) and the advective mixed-layer model (AKT, solid curves); and (b) the temperature $\bar{T}_s$ of the mixed layer. Integration is over a four-year period and WS and SS denote winter and summer solstices on the abscissa.

### *a. Meridional and vertical eddy fluxes*

#### 1) ZONALLY AVERAGED MOTIONS

The transportations by the zonally averaged motions are calculated explicitly and may be obtained from the $\bar{M}(\bar{X})$ in (5). For example, using (3) we may define the meridional flux of momentum by the zonally averaged quantities as

$$\langle u\rangle\langle v\rangle=(1/4\pi^2)\Big[\sum_{k=1,K}(\lambda_k-\lambda_{k-1})\bar{u}_k\Big]\Big[\sum_{k=1,K}(\lambda_k-\lambda_{k-1})\bar{v}_k\Big], \tag{16}$$

which for the two domains of equal longitudinal extent (see Fig. 2), becomes

$$\tfrac{1}{4}[\bar{u}\bar{v}+\tilde{u}\tilde{v}+\bar{u}\tilde{v}+\tilde{u}\bar{v}], \tag{17}$$

where the barred quantities represent domain averages over the atmospheric domain A1 and quantities demarked by the tilde denote domain averages over A2. The convergences of mean momentum and heat flux by the zonally averaged motions are shown in Figs. 11 and 12 for both converged equinox and solstice cases. The distributions will be discussed presently along with other results from the two convergence experiments.

#### 2) TRANSIENT EDDIES

As distinct from the heat and momentum transportations by the mean meridional motions, the fluxes by the deviations from the domain averages require an implicit treatment. That is, the determination of the $\bar{D}(X')$ terms require the expression of the eddy momentum, heat and moisture fluxes ($\overline{u'v'}$, $\overline{v'v'}$, $\overline{u'\omega'}$, $\overline{v'\omega'}$, $\overline{v'T'}$, $\overline{\omega'T'}$, $\overline{v'q'}$ and $\overline{\omega'q'}$) in terms of the domain averaged quantities of each domain (e.g., $\bar{u}$, $\bar{v}$, $\bar{\omega}$, etc.).

To achieve a closure and thus represent the transient eddies in terms of the mean variables, we closely follow Green (1970), Saltzman and Vernekar (1971), Stone (1973 and 1974) and Wiin-Nielson and Sela (1971). The applicability of these parameterization schemes will be discussed in the last section of the paper.

We list the various parameterizations, referring the reader to the cited references for further details. An expression for the meridional and vertical fluxes of heat is given by (Stone, 1974)

$$\left.\begin{aligned}\overline{v'T'}&=-A^*(\bar{\theta}_y+B\bar{\theta}_z)\\ \overline{\omega'T'}&=B^*(\overline{v'T'})\end{aligned}\right\}. \tag{18}$$

Similar expressions are assumed for quasi-conservative quantities such as specific humidity except that $\bar{\theta}$ is replaced by $\bar{q}$. The lateral transport of eddy momentum is represented in terms of the transport of mean quasi-geostrophic potential vorticity such that (Green, 1970, Wiin-Nielson and Sela, 1971)

$$\frac{(\overline{u'v'}\cos^2\phi)_\phi}{a\cos^2\phi}=-A^*(\bar{\gamma}_y+B^*\bar{\gamma}_z)+\left(\frac{f_0R}{\sigma p}\overline{v'T'}\right)_p, \tag{19}$$

where $\overline{v'T'}$ is provided by (18) and the mean potential vorticity is defined by

$$\bar{\gamma}=f-\bar{u}_y-(f_0\rho\bar{\theta}\bar{\theta}_p^{-1}\bar{\psi}_p)_p,$$

where $\psi$ is a streamfunction. Expressions for the squared eddy quantities may be written as (Saltzman and Vernekar, 1971)

$$\bar{v}'^2=\frac{\overline{v'T'}\nu}{(1-\epsilon)(\partial\bar{T}/\partial y)}, \tag{20}$$

where $\overline{v'T'}$ is provided by (18) and $\epsilon=0.25$, a factor which accounts for adiabatic heating and cooling.

In the above expressions, $A^*$ and $B^*$ are transfer coefficients defined by

$$\left.\begin{aligned} A^*&=\frac{0.144R}{f^2a}\left(\frac{p}{p_0}\right)^{\kappa}(-p\bar{\theta}_p)^{\frac{1}{2}}\bar{\theta}_y f(z)\\ B^*&=-\bar{\theta}_y\left(\frac{p}{p_0}\right)^{\kappa}[2.5(-p\bar{\theta}_p)^{-1}+1.42(|\bar{\theta}_y|)^{-1}]g(z)\end{aligned}\right\}, \tag{21}$$

where $f(z)$ and $g(z)$ are functional height distributions, $P_0=1000$ mb, $\bar{\theta}$ represents the domain-averaged potential temperature and $\nu$ is the frequency of the assumed periodic baroclinic motions.

Utilization of (18)–(21) allows the calculation of the $\bar{D}(X')$ terms of (6), subject to the approximations inherent in the parameterizations, the validity of which are discussed in Section 6.

### b. *Interdomain fluxes and interaction terms*

The formulation of a parameterization representing the east-west (or zonal) fluxes and pressure gradient terms represents an integral part of the model development as it is by these processes that the domains communicate and interact. Earlier we saw that the domain averaging process results in the evaluation of point quantities at the boundaries of the domains. In the following processes we will present a first attempt to achieve a consistent parameterization of the $\bar{I}(X)$ terms of (7) as functions of the mean variables of the domain structure. The degree to which the particular parameterization represents real processes in the atmosphere will be discussed in Section 6.

If we define a mean basic state such that

$$f\langle u\rangle=-(1/a)\langle\psi\rangle_\phi, \tag{22}$$

where the angle braces represent a zonal average as defined in (3), we can linearize the horizontal momentum equations about such a base state. If the primed quantities denote deviations about (22), the horizontal momentum equations become

$$u'_t+\frac{\langle u\rangle}{a\cos\phi}u'_\lambda+\frac{v'}{a}\langle u\rangle_\phi=-\frac{1}{a\cos\phi}\psi'_\lambda+fv'-Du' \tag{23}$$

$$v'_t+\frac{\langle u\rangle}{a\cos\phi}v'_\lambda=-\frac{1}{a}\psi'_\phi-fu'-Dv', \tag{24}$$

where $D$ represents some dissipative coefficient. If we assume that the perturbations possess a functional form

$$X(\lambda,\phi,p)=\mathrm{Re}\sum_s X(\phi,p)\exp i(s\lambda-\nu t), \tag{25}$$

(23) and (24) can be solved for $u$ and $v$ in terms of $\psi$ ($s$ is a nonzero integer to be defined). Manipulation yields

$$u=[(a_1-ia_2)\psi-a_3\psi_\phi]b, \tag{26}$$

$$v=[ia_4\psi-(a_5+ia_6)\psi_\phi]b, \tag{27}$$

where

$$\left.\begin{aligned} a_1&=\frac{s^2\langle u\rangle}{(a\cos\phi)^2}, & a_2&=\frac{Ds}{a\cos\phi}\\ a_3&=\frac{1}{a}\left(f-\frac{\langle u\rangle_\phi}{a}\right), & a_4&=\frac{fs}{a\cos\phi}\\ a_5&=\frac{D}{a}, & a_6&=\frac{\langle u\rangle s}{(a\cos\phi)^2}\\ b&=\left[fa_3+D^2-\left(\frac{\langle u\rangle s}{a\cos\phi}\right)^2+\frac{2iDs\langle u\rangle}{a\cos\phi}\right]^{-1}\end{aligned}\right\}.$$

In the derivation of (26) and (27) we have made the assumption that

$$\nu\ll\frac{\langle u\rangle s}{a\cos\phi}, \tag{28}$$

which states that the longitudinal advective time scale is much shorter than the modal period. In other words, we are assuming quasi-stationary solutions, which carries with it the tacit assumption that the majority of the meridional eddy fluxes are accomplished by the large-scale quasi-stationary eddies, which possess time scales determined by the slowly evolving state of the land and ocean domains. Substitution of (26) and (27) into (25) allows the relation of the perturbation quantities $u'$, $v'$ and $\psi'$ in terms of $\psi$. The definition of a closure assumption, which relates $\psi$ to the mean domain variables, will define fields of $u'$, $v'$ and $\psi'$ from which point values of the variables can be evaluated at the boundaries of the domain, thus allowing the evaluation of the $\bar{I}(X)$ of (7).

We accomplish the specification of the geopotential by assuming that the geopotential may be written in the functional form

$$\psi(\phi,p)=\Delta\psi(\phi,p)\exp i\gamma(\phi,p). \tag{29}$$

Here we have merely defined $\psi$ to isolate the magnitude of the geopotential perturbation $\Delta\psi$ and a latitude-dependent and height-dependent phase function $\gamma$.

With the definition of the form of $\psi$ in (29) we obtain the following representation of the perturbation velocity

component fields:

$$u'=\mathrm{Im}\sum_s\left[(a_1-ia_2)\Delta\psi-a_3(\Delta\psi_\phi+i\gamma_\phi\Delta\psi)\right]b \times\exp i(s\lambda+\gamma), \quad (30)$$

$$v'=\mathrm{Im}\sum_s\left[ia_4\Delta\psi-(a_5+ia_6)\Delta\psi_\phi+(a_6-ia_5)\gamma_\phi\Delta\psi\right]b \times\exp i(s\lambda+\gamma). \quad (31)$$

If the value of $s$ in (25) is determined to be the maximum resolvable longitudinal mode, given the total number of domains at any latitude circle, the magnitude functions $\Delta\psi_s$ emerge from the Fourier analysis of the mean longitudinal structure which is represented by the mean domain geopotentials themselves. In the two domain system shown in Fig. 2, where each domain is of equal longitudinal extent, we require only one magnitude function which is for the $s=1$ mode, *viz.*,

$$\Delta\psi_{s=1}=\bar{\psi}_{k=2}-\bar{\psi}_{k=1}. \quad (32)$$

For a higher number of domains, or for a system in which the domains are of unequal size, a higher order expansion in $s$ is required. For example, in a two-domain system where one domain extends from 0 to $3\pi/2$ and the second from $3\pi/2$ to $2\pi$, $\Delta\psi_{s=1}$ and $\Delta\psi_{s=2}$ are resolvable along with a residual which may be attributed to higher modes.

The term $\gamma(\phi,p)$ describes the variation of the vertical tilt with height and latitude of the parameterized longitudinal structure. Once again assuming slowly varying or stationary behavior, manipulation of the quasi-geostrophic vorticity equation, together with the thermodynamic and continuity equations, all linearized about the basic state defined in (22), yield the following expression in the perturbation meridional velocity component $v'$:

$$v'_{pp}+\frac{1}{\langle u\rangle}\left(\frac{\sigma\beta}{f_0^2}-\langle u\rangle_{pp}\right)+\frac{\sigma}{f_0^2}\nabla^2v'=-\frac{R}{C_pf_0\langle u\rangle}\left(\frac{\dot{Q}}{p}\right)_p. \quad (33)$$

If we assume a simple heating function which decreases fairly rapidly with height above the ground, the vertical structure of the forced mode will approximate that of the free mode with increasing height (i.e., as $\dot{Q}$ approaches zero). If we are prepared to assume such a structure in $\dot{Q}$ and allow only a linear shear in $\langle u\rangle$, (33) reduces to

$$v'_{pp}+\frac{\sigma\beta v'}{f_0^2\langle u\rangle}+\frac{\sigma}{f_0}\nabla^2v'=0,$$

which separates if we set

$$v'(\phi,\lambda,p)=V(p)\exp i(s\lambda+l\phi), \quad (34)$$

producing the vertical structure equation

$$V_{pp}+\left[\frac{\sigma\beta}{f_0^2\langle u\rangle}-\frac{\sigma}{f_0^2}(s^2+l^2)\right]V=0$$

which possesses solutions of the form $V(p)\propto\exp(imp)$ if

$$m^2=\frac{\sigma}{f_0^2}\left[\frac{\beta}{\langle u\rangle}-(s^2+l^2)\right]. \quad (35)$$

In the longitude-height plane, such a mode possesses vertical phase shifts given by

$$\frac{d\lambda}{dp}=\frac{m}{s}=\frac{1}{s}\left(\frac{\sigma}{f_0}\right)^{\frac{1}{2}}\left[\frac{\beta}{\langle u\rangle}\left(1-\frac{s^2+l^2}{\beta}\langle u\rangle\right)\right]^{\frac{1}{2}}. \quad (36)$$

Eq. (36) provides a measure of the *relative* phase shift of a forced mode (under the assumption of a rapidly decaying $\dot{Q}$) in the vertical as a function of latitude and wavenumber. The *absolute* phase function $\gamma(\phi,p)$ is given as

$$\gamma(\phi,p)=\gamma_0+d\lambda/dp, \quad (37)$$

where $\gamma_0$ is a free parameter relating the wave to the position of the maximum longitudinal forcing; it was determined by assuming that the 750 mb trough was 30° west of the surface trough.

The dissipation coefficient $D$ in (23) and (24) is assumed to have the latitudinal structure

$$D=D_0\{1+\exp[(\phi-\phi_c)/\Delta\phi_D]\}, \quad (38)$$

where $\phi_c=20°$ and $\Delta\phi_D=8°$ so that the frictional effect reduces rapidly to zero outside the $\pm20°$ latitude belt and reaches a maximum near the equator. Such a dissipative parameterization avoids excessive damping at high latitudes and allows for large dissipation ($D_0=1.5\times10^{-5}$ s$^{-1}$) which has been indicated by Holton and Colton (1972) to be necessary in order to achieve a realistic simulation of large-scale tropical motions. Holton and Colton rationalized that the large dissipation was a result of the drag associated with cumulus activity.

The closed perturbation fields defined in the last paragraphs possess limits which allow some insight into the parameterization. Considering the coefficients of (26) and (27) for ultra-large-scale motions in mid-latitudes, the following scales are suggested:

$$f\gg\frac{1}{a}\langle u\rangle_\phi\approx\frac{s\langle u\rangle}{a\cos\phi}\gtrsim\frac{Ds}{a\cos\phi},$$

which infers an ordering of the coefficients such that

$$a_3\approx a_4,\ a_3\gg a_1 \text{ and } a_4\gg a_5 \text{ and } a_6;$$

and as $b\approx f^{-2}$, Eqs. (30) and (31) are approximated by

$$u'\approx-\frac{1}{fa}(\Delta\psi)_\phi\sin(s\lambda+\gamma), \quad (39)$$

$$v'\approx-\frac{fs}{a\cos\phi}\Delta\psi\cos(s\lambda+\gamma). \quad (40)$$

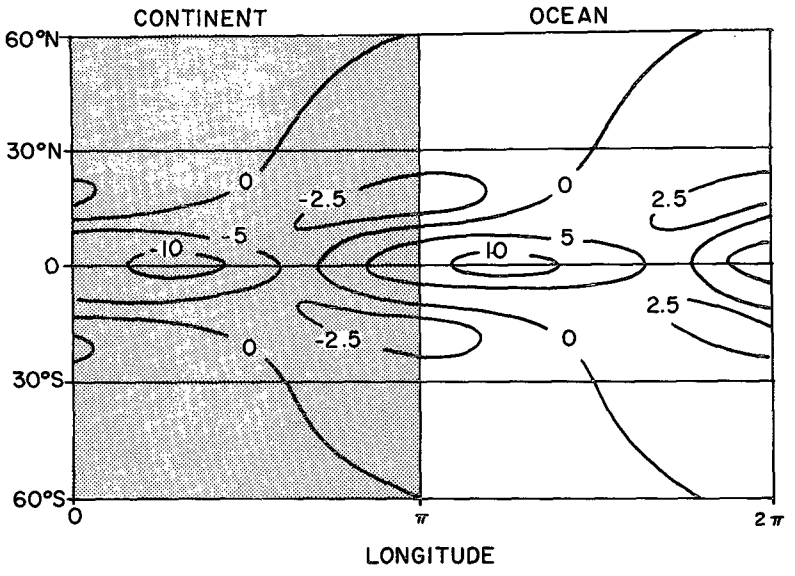


FIG. 6. Perturbation vertical velocity distribution at 500 mb for the simple domain structure shown in Fig. 1 at an equinox. Units are $10^{-4}$ mb $s^{-1}$.

Eqs. (39) and (40) define an approximate geostrophic state expressed as functions of the domain-averaged geopotential field defined in (32). Near the equator the scalings

$$a_2 > a_1 \gg a_3 \text{ and } a_5 > a_6 \gg a_4$$

become apparent, reflecting the diminishing value of $f$ and the weakening of the mean geopotential gradients near the equator. Then as $b \approx D^{-2}$ at low latitudes, (30) and (31) are approximated as

$$u' \approx -\frac{\Delta\psi}{Da\cos\phi}\cos(s\lambda+\gamma), \tag{41}$$

$$v' \approx -\frac{1}{Da}(\Delta\psi)_\phi \sin(s\lambda+\gamma). \tag{42}$$

Eqs. (41) and (42) indicate a structure in which the meridional perturbation velocity component approaches zero near the equator so the flow must be restricted to the zonal plane. Also, at low latitudes the phase shift in the vertical approaches 180° through the troposphere. Such a state is similar to that observed for the mean seasonal tropical atmosphere by Krishnamurti (1971) or suggested theoretically by Webster (1973).

The structure of the perturbation field is best demonstrated by considering the associated $\omega$ field (i.e., $dp/dt$) at the 500 mb level (shown in Fig. 6). The mean domain structure upon which the perturbation field depends comes from the converged equinox case which will be discussed in Section 5. The $\omega$ field indicates intense rising motion over the low-latitude continental region with equally intense subsidence over the equatorial ocean. Eqs. (41) and (42) suggest that the flow is nearly two-dimensional. Toward middle latitudes the intensity of the vertical motion decreases and regions of ascent are principally over ocean regions. Such a distribution will be found to be consistent with the surface temperature distributions for equinox conditions (which is shown in Fig. 16).

The final form of the zonal flux and interdomain interaction terms is reached by defining a decomposition of a quantity $X$ such that

$$X = \langle X\rangle + X', \tag{43}$$

where $X'$ represents the perturbation quantities defined in (30) and (31) relative to the definitions (32) and (37). We may calculate $\bar{I}(\lambda)$, for example, by introducing (43) into (7). This provides

$$\bar{I}(\lambda) = -\frac{1}{a\cos\phi}[(\langle u\rangle+u')_\pi{}^2 - (\langle u\rangle+u')_0{}^2 - (\langle\psi\rangle+\psi')_\pi + (\langle\psi\rangle+\psi')_0]d_k,$$

and as $X'_\pi = X'_0$ for the two equal sized domain case, we obtain

$$\bar{I}(\lambda) = -\frac{1}{a\pi\cos\phi}(4\langle u\rangle u'_0 + 2\psi'_0). \tag{44}$$

In a similar manner the remaining terms of (7) reduce to

$$\bar{I}(\phi) = -\frac{2}{\pi a\cos\phi}(\langle u\rangle v'_\pi + \langle v\rangle u'_\pi), \tag{45}$$

$$\bar{I}(T) = -\frac{2}{\pi a\cos\phi}(\langle u\rangle T'_\pi + \langle T\rangle u'_\pi), \tag{46}$$

$$\bar{I}(q) = -\frac{2}{\pi a\cos\phi}(\langle u\rangle q'_\pi + \langle q\rangle u'_\pi) \tag{47}$$

$$\bar{I}(m) = -\frac{2}{\pi a\cos\phi}u_\pi. \tag{48}$$

TABLE 1. Coefficients and constants used to specify the two-layer domain-averaged model.

| | | |
|---|---|---|
| Incident solar radiation | $S$ | 328 W m$^{-2}$ |
| Coefficient of horizontal eddy conductivity | $A_{H,T}$ | $4\times10^{5}$ m$^2$ s$^{-1}$ |
| Roughness parameter | $z_0$ (ocean) | $10^{-2}$ m |
| | $z_0$ (land) | $10^{-1}$ m |
| Height of constant flux layer | $h$ | 80 m |
| Depth of penetration of shortwave radiation into ocean | $\beta$ | 10 m |
| Emmissivity of atmosphere | $\epsilon$ | 1.02 |
| Atmospheric absorbtivity to longwave radiation | $a$ | 0.96 |

The distribution of the interdomain terms will be presented in Section 5 for solstice and equinox conditions.

## 4. Heating, dissipation and subgrid-scale processes

The basic driving mechanism of the model is the heating and cooling of the system created by the difference between the incoming solar radiation and the outgoing terrestrial radiation. The simple radiative transfer model we will adopt is that introduced by Charney (1959). The atmosphere is assumed to be isothermal, transparent to incoming solar radiation and partially absorbing of terrestrial radiation. Over continental regions we assume zero heat capacity while oceanic regions are assumed to possess a large heat capacity. This results in a difference in the determination of surface temperature over land and ocean regions. Over land an energy balance method is utilized in the manner described below. Over the ocean, the surface temperature is determined by the advective mixed-layer model (Section 2b) which depends upon both an energy balance at the surface of the ocean, the internal and wind induced mixing within the layer itself, the deep ocean temperature structure, and the latitudinal advection resulting from the large-scale circulation.

A constant flux layer of depth $h$ (assumed to be 80 m) is assumed to represent the lower boundary of each domain. To calculate a quantity at height $h$ we assume that the flux from the lower surface can be described in terms of an eddy diffusion coefficient. We can write

$$-\mu\frac{\partial T}{\partial z}=-\frac{\mu}{\Delta z}(T_1-T_h)=\rho C_D|V_0|(T_0-T_h),$$

so that

$$T_h=\frac{nT_0+T_1}{n+1}, \tag{49}$$

where $n=\rho\Delta z C_D|V_0|/\mu$. Here $V_0$ is the velocity at the lower boundary and is assumed to be half the velocity at 750 mb, which is the first prognostic layer in the model, and $C_D$ is a drag coefficient defined by

$$C_D=\left[\frac{K_0}{\ln(h+z_0)/z_0}\right]^2,$$

where $z_0$ is a roughness parameter and $K_0$ is von Kármán's constant.

The surface temperature over land is given by the solution of the energy balance equation

$$S_0+I_D=\sigma T_0^4+F_S+F_L+F_I. \tag{50}$$

Here $S_0$ refers to the incoming solar radiation at the surface of the earth which is given by

$$S_0=(1-\alpha)S(\tfrac{1}{2}\pi\sin\phi\sin\delta+\cos\phi\cos\delta), \tag{51}$$

where $\delta$ is the solar declination angle, $\phi$ the latitude, $S$ the incident solar radiation at the outside of the atmosphere and $\alpha$ the systems albedo. The longwave atmospheric reradiation is given by

$$I_D=\epsilon\sigma T_M^4=\epsilon\sigma[\tfrac{1}{2}(T_1+T_2)]^4, \tag{52}$$

where $T_M$ is the mean atmospheric temperature of the atmospheric column, $T_1$ and $T_2$ are the atmospheric temperatures at 750 and 250 mb, the two prognostic levels of the model, and $\epsilon$ is the emmissivity.

$F_S$ and $F_L$ represent the sensible and latent heat fluxes at the lower boundary. Consistent with the constant flux layer parameterization, $F_S$ is defined as

$$F_S=(g/\Delta p)C_D\rho_0|V_0|(T_0-T_h), \tag{53}$$

where $T_h$ is defined in (53) and $T_0$ in (50). In the simple experiments described in the next section, we will not include a hydrology cycle. Consequently we set

$$F_L=0 \tag{54}$$

and in the absence of a cloud-albedo feedback we follow Faegre (1972) and define $\alpha$ as a slowly varying function of temperature such that

$$\alpha=0.486-0.0092(T_0-273) \tag{55}$$

for $0.2<\alpha<0.8$.

The surface temperature in the ocean domain when there is sea ice is calculated from (50). $F_I$ represents the heat flux through the ice from the warmer ocean to the cooler atmosphere. Such a flux is inversely proportional to the ice thickness $h_I$ and is given by

$$F_I=(k/h_I)(T_s-T_I), \tag{56}$$

where the ice thickness possesses the analytic thickness distribution from the latitude $\phi_c$ of ice formation which is given by

$$h_I=2h_c\left[1-\frac{1}{2}\left(\frac{\cos\phi}{\cos\phi_c}\right)^2\right]. \tag{57}$$

$T_I$ is the freezing temperature of sea water and $k$ the heat conductivity of sea ice; $h_c$ is assumed to be 0.5 m.

To obtain expressions for frictional dissipation, we follow Bates (1972) and write the total dissipative force as

$$\mathbf{F}(\phi,\lambda,p)=-g\frac{\partial\tau}{\partial p}+A\nabla_h^2\mathbf{V}, \tag{58}$$

where for the interior of the atmosphere we may write

$$\tau=\mu\frac{\partial\mathbf{V}}{\partial z}$$

while at the lower boundary, we have

$$\tau=C_D\rho|\mathbf{v}_0|\mathbf{v}_0.$$

Assuming a two-layer formulation, we can use (58) to write $F_1$ of (1) at each level as

$$\left.\begin{aligned}F_1(1)&=k(\bar{u}_2-\bar{u}_1)+\frac{A}{a}\frac{\partial}{\partial\phi}D(\bar{u}_1)-\frac{g}{\Delta p}C_D\rho_0|u_0|u_0\\F_1(2)&=k(\bar{u}_1-\bar{u}_2)+\frac{A}{a}\frac{\partial}{\partial\phi}D(\bar{u}_2)\end{aligned}\right\}. \tag{59}$$

Here $D=(1/a\cos\phi)(\partial/\partial\phi)[(\ )\cos\phi]$ and $k=g\mu/\Delta p\Delta z$. Similar expressions exist for $F_2$ in (1). The subscripts 1 and 2 on the right-hand side refer to the 750 and 250 mb level, respectively, and $\Delta z$ corresponds to the thickness between the two levels.

By the same procedure we can specify $F_3$ for the two layer model as

$$\left.\begin{aligned}F_3(1)&=-k_T\delta T+\frac{A}{a}\frac{\partial}{\partial\phi}D(\bar{T}_1)+F_s+F_L\\F_3(2)&=-k_T\delta T+\frac{A}{a}\frac{\partial}{\partial\phi}D(\bar{T}_2)\end{aligned}\right\}, \tag{60}$$

where

$$\delta T=\begin{cases}(\bar{T}_1-\bar{T}_2)-\dfrac{g}{C_p}\Delta z, & \text{for}\quad (\bar{T}_1-\bar{T}_2)\geqslant\dfrac{g}{C_p}\Delta z\\ 0, & \text{otherwise.}\end{cases}$$

As we will consider only the dry atmosphere, we need not specify $F_4$ in (1). In the absence of moist processes the difference between the oceanic and the land domains reduces to that which arises from different radiative properties, drag coefficients and lag times to changes in incoming solar radiation which may result from the manner in which the surface temperature is determined in each domain. A further difference occurs in the assumed value of the roughness parameter $z_0$ which is set an order of magnitude smaller for the ocean than the land. The effect of this is to reduce the oceanic drag coefficient by a factor of 2. The various parameters which define the domain structures are shown in Table 1.

## 5. Simple experiments

In order to assess the capability of the model in simulating a joint atmosphere-ocean system, two simple experiments were performed using the simplest prototype of the domain-averaged model. Here the model was reduced to two atmospheric domains (Fig. 2), one residing over a pole-to-pole land mass of $\pi$ radian extent in longitude and the other over a mixed-layer ocean, as described in Section 2b. The atmospheres were divided into two vertical layers plus the simple constant flux boundary layer described in the last section. Such specialization, together with the numerical schemes employed, is discussed in an Appendix.

In the first experiment the model was run from rest and with each layer assumed to be independently isothermal. The radiative heating was assumed to have an equinoctial distribution. In the second experiment the procedure was repeated, but the radiative heating possessed a Northern Hemisphere summer solstice distribution. Each experiment was continued until converged solutions were achieved.

In the discussion to follow, it should be remembered that the results represent *converged* equinoctial and solsticial fields and not *mean* or *average* fields which would result from averaging the results of an evolving or transient model over a time period of (say) one month. The differences between these two result-types are nontrivial and evolve from the varied time scales associated with the various physical processes. In the real atmosphere (or in a transient atmosphere-ocean model), the ocean surface temperature lags significantly behind its counterpart over the land in the subtropics and mid-latitudes and occurs some six weeks or so after the summer solstice and when the insolation is decreasing fairly rapidly.

By allowing the model to approach an equilibrium solution for a prescribed and fixed solar heating a quite different solution is achieved from that described above. This is because the system will *not* assume a converged solution until the sea surface temperature has ceased to change, i.e., until the longest time scale in the system has been surpassed. Consequently, as the insolation is held constant, the maximum sea surface temperature has time to catch up with the maximum land surface temperature. The product of these two incorrectly phased processes will be to produce a solution quite different from that observed in the real atmosphere or from that produced by an ocean-atmosphere model forced by a properly varying insolation.

Such deviations from reality have been avoided by many general circulation models by using the appropriate climatological sea-surface temperature which appears as a fixed lower boundary condition. The paradoxical consequence of this is that for a perpetual July simulation, for example, the results will be closer to reality for a general circulation model *without* an

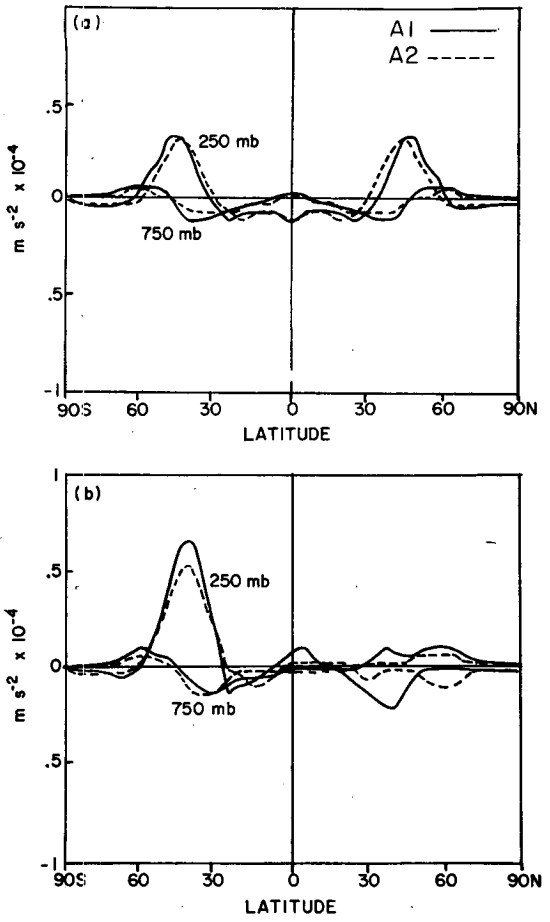


FIG. 7. Latitudinal convergence of westerly momentum by the transient eddies for the atmospheric domain over land (A1, solid curves) and the atmospheric domain over the ocean (A2, dashed curves) at the 250 and 750 mb levels for (a) the equinox and (b) the solstice.

interactive ocean, but with a fixed climatological sea surface temperature, than for a model with an interactive ocean which is allowed to run to a statistical steady state. However, only the latter model will contain the necessary physics and time-scale interaction that will allow the approach of a proper simulation of the system evolution through an annual cycle, or longer, as considered by Lau and Webster (1977).

### *a. The converged flux fields*

The flux of heat and momentum by the various processes described in Eqs. (5)–(7) are shown in Figs. 7–12 for both the converged equinox and Northern Hemisphere summer solstice. In all diagrams the panel marked (a) refers to the equinox case, whereas (b) refers to the solstice. The solid curves, unless otherwise specified, refer to the A1 domain while the dashed lines refer to the A2 domain. All quantities are shown in convergence form.

Figs. 7 and 8 show the latitudinal convergence of momentum and heat flux by the transient eddies as described by the parameterizations (18)–(21). For both quantities a significant difference is apparent between the two domains. The maximum convergence of both heat and momentum is slightly equatorward and smaller over the ocean (A2) than over the continent (A1)—features which are traceable to the mean structure in each domain (see especially Figs. 16a and 16b). The solstice case shows similar differences occurring between the two domains with the general feature of maximum convergence occurring in the winter hemisphere. Each distribution possesses comparable magnitudes and distributions to the mean zonal statistics calculated by Oort and Rasmusson (1971). For example, the maximum momentum convergence occurs poleward of the maximum westerly wind or in a similar location to the angular velocity maximum.

Figs. 9 and 10 show the zonal or interdomain convergence of momentum and heat flux for each season *into* the atmospheric domain over the continent (i.e., A2 to A1). In both seasons the momentum flux convergence is roughly a factor of 2 or 3 smaller than the latitudinal flux convergence shown in Fig. 7, and also

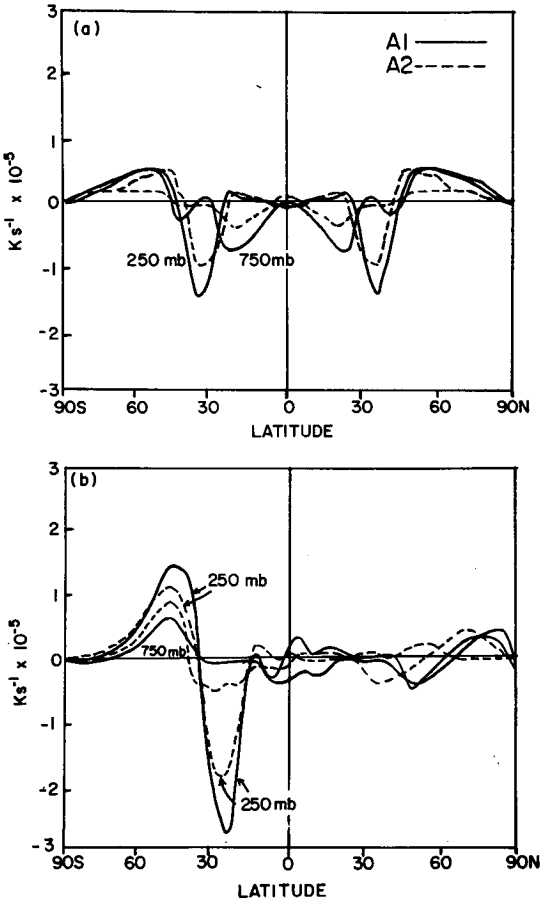


FIG. 8. As in Fig. 7 except for the latitudinal convergence of heat flux.

possesses a different distribution. At the equinox, strong interdomain interaction is evident, especially in the low latitudes, where a momentum convergence distribution, consistent with a near equatorial zonal circulation, occurs with compensating momentum convergence appearing between the upper and lower troposphere. The solstice distribution shows quite a different arrangement with a strong convergence of westerly momentum occurring in the middle latitudes of the summer hemisphere. The maximum at 250 mb coincides with the maximum upper tropospheric westerlies shown in Fig. 13b.

The zonal heat flux convergence fields of Fig. 10 also possess interesting and significant distributions. Like the momentum convergence, the magnitudes are about a factor of 3 or so less than the latitudinal flux convergences at the equinox. Large values occur in the solstice case at 750 mb, however, with a strong convergence of heat into the ocean region. The magnitude is similar to that of the heat flux convergence by the transient eddies in the winter hemisphere (Fig. 8b) and suggests a heating rate of near 1.5 K day$^{-1}$. The location

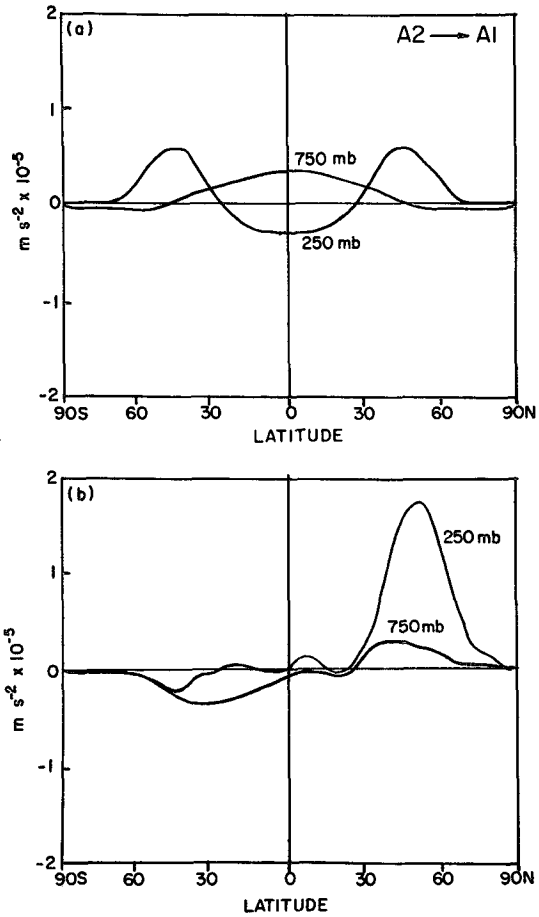


FIG. 9. Longitudinal convergence of westerly momentum *into* the atmospheric domain over the land (A1) at the 250 and 750 mb levels for (a) the equinox and (b) the solstice.

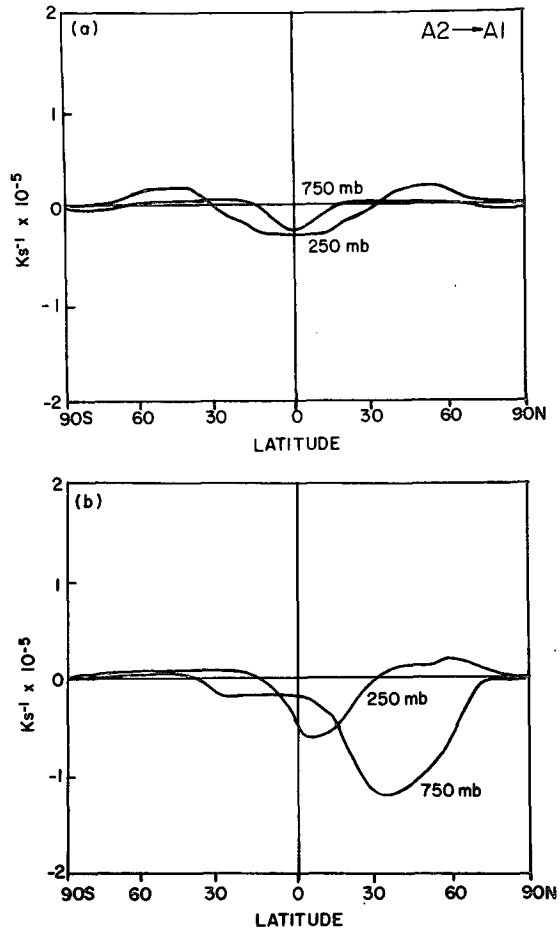


FIG. 10. As in Fig. 9 except for the longitudinal convergence of heat flux.

corresponds to the maximum temperature difference at 750 mb (Fig. 16b).

The convergence of momentum and heat flux by the mean meridional circulation of the model for the two seasons are shown in Figs. 11 and 12. Quantities relating to the mean meridional circulation were calculated by averaging the quantities from each domain in the manner described in (17). The mean convergence distributions seem consistent with the meridional velocity component distributions shown in Figs. 14a and 14b with maximum flux convergence occurring in the subtropics, somewhat equatorward of the eddy flux convergence maxima. The heat flux convergence patterns shown in Fig. 12b indicate a strong cross-equatorial transport of heat away from the summer hemisphere in the upper troposphere. This flux emanates from a strong divergent region near 25°N. A strong heat transport into the summer hemisphere occurs in the lower troposphere. Averaged in the vertical the total flux convergence is very small, although, redefined in the manner of Oort and Rasmusson (1971) where the

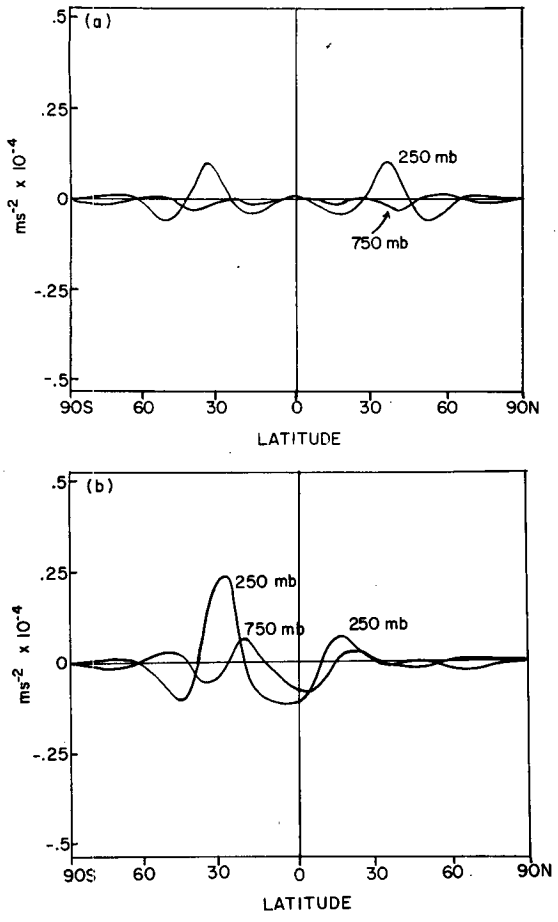


FIG. 11. Latitudinal convergence of westerly momentum by the total mean meridional motions at the 750 and 250 mb levels for (a) the equinox and (b) the solstice.

temperature anomaly in the vertical is used rather than absolute temperature, the magnitudes are quite similar.

In summary, it would appear that all three flux forms act as strong modifiers and redistributors of heat and momentum. Importantly, the interdomain fluxes and interaction terms are significant and generally only a factor of 2 smaller than the north-south eddy fluxes. Consequently, each domain is a strong function of its neighbor and the time scales of one part of the system (e.g., the ocean domain) will be imprinted upon the character of the other, and vice versa, via the interdomain terms.

### *b. The converged mean domain fields*

The various mean domain fields are shown in Fig. 13–17 for both the converged equinox and Northern Hemisphere summer solstice. Solid curves refer to domain A1 and the dashed curves to A2. The surface temperature [marked $\bar{T}$ (1000 mb)] pertaining to the A2 domain (A2) curve is the same as the ocean mixed-layer temperature $\bar{T}_s$. (The depth of the mixed layer is shown for both seasons in Fig. 17.)

The zonal wind fields are presented in Fig. 13. At the equinox strong upper tropospheric westerlies are symmetrically situated about the equator with the A1 magnitude stronger by 3 m s$^{-1}$ than the corresponding value over the ocean and with a position slightly poleward. Weaker westerlies prevail in the lower troposphere. Nearer the equator, fairly strong low-level easterlies are evident and these are strongest over the ocean. At the Northern Hemisphere solstice, a completely different zonal wind field develops with the winter hemisphere being dominated by much stronger westerlies (~43 m s$^{-1}$) which are considerably equatorward of their equinox positions. In the winter subtropics the low-level easterly flow is also somewhat stronger and similarly removed toward the equator. The largest changes over land occur in the summer hemisphere, however, with the upper tropospheric subtropics being dominated by a strong easterly maximum (~ −24 m s$^{-1}$ at 250 mb) which lies over fairly strong low-latitude and subtropical westerlies. Over the ocean (A2) a broad easterly flow dominates most of the summer hemisphere at 750 mb below a moderate westerly flow.

The role of the east-west fluxes and interaction terms,

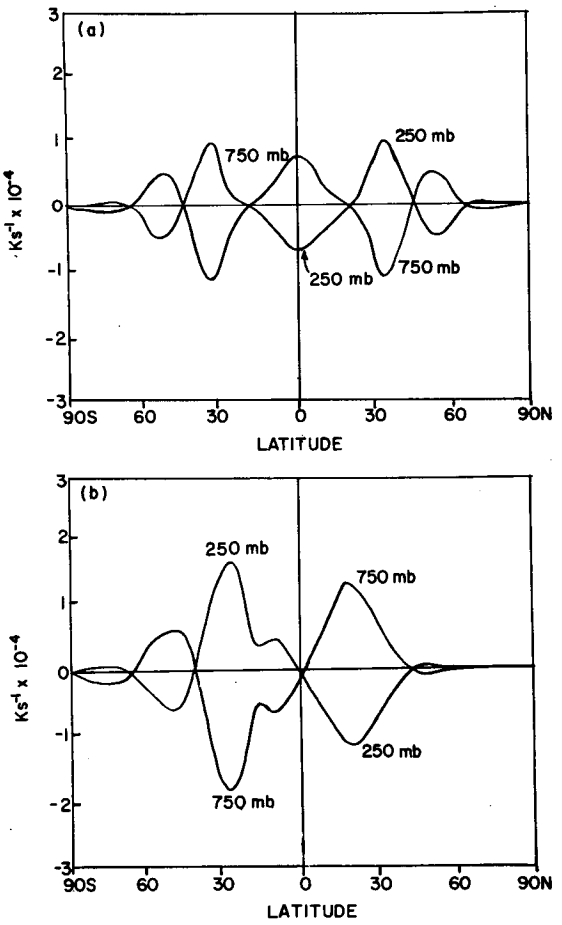


FIG. 12. As in Fig. 11 except for the convergence of heat flux.

which are described in (7) and shown in Figs. 9 and 10, was assessed by running two separate *one-domain* experiments (i.e., two zonally averaged experiments), one with a lower boundary condition of continental character and the other with a lower boundary condition determined by the ocean model. With the absence of the interdomain terms, the fields differed markedly from those shown in this paper. In particular, the magnitudes of the zonal wind extrema were larger in the continental case and smaller in the ocean case. Furthermore, the relative positions were further apart in latitude than shown in Fig. 13. This is to be expected from the magnitudes of the interdomain heat and momentum fluxes shown in Figs. 9 and 10. It would seem that the interdomain effects (or the distribution of land and ocean) act as strong secondary determiners of the mean domain structure.

The meridional velocity field at 250 mb is presented in Fig. (14) and the vertical velocity at 500 mb in Fig. 15. At the equinox both domains possess strong Hadley-type circulations in the equatorial and sub-

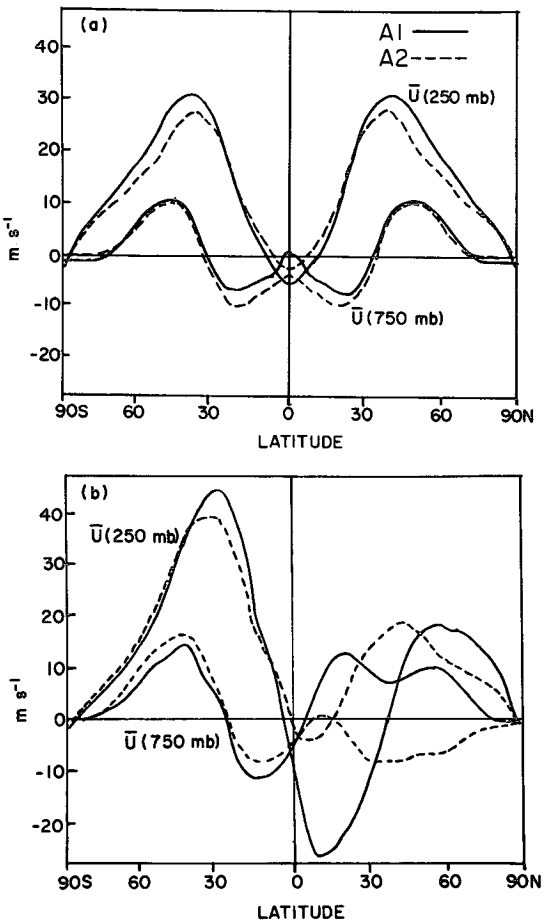


FIG. 13. Latitudinal distribution of the zonal wind component for the atmospheric domain over land (A1, solid curves) and the atmospheric domain over the ocean (A2, dashed curves) at 750 and 250 mb for (a) the equinox and (b) the solstice.

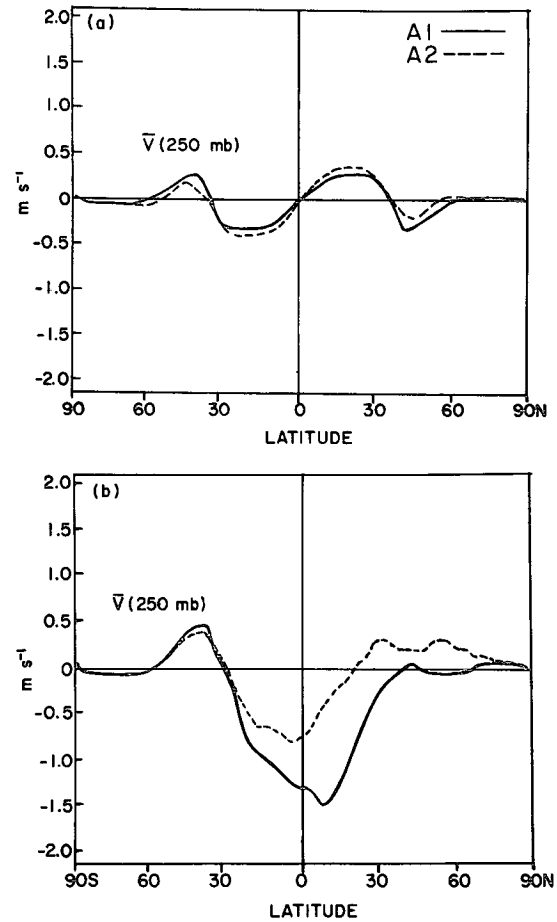


FIG. 14. As in Fig. 13 except for the mean meridional velocity component at 250 mb.

tropical regions and weaker reverse mid-latitude cells. The latter probably originate from the inclusion of the north-south eddy flux parameterizations as a residual circulation. The stronger mid-latitude cell over the land is consistent with the temperature structure shown in Fig. 16 and with the stronger westerlies shown in Fig. 13. This is because the momentum flux is effectively a function of the quasi-geostrophic potential vorticity gradient which depends partially upon the latitudinal gradient of $\bar{u}_y$. The difference between the strength of the Hadley cells in the two domains is less than that between the two mid-latitude cells. This is probably due to the strong east-west momentum flux compensation between the two domains which may be seen in Fig. 9a. The vertical velocity distributions of Fig. 10 appear to be consistent (i.e., from continuity) with the meridional velocity fields of Fig. 9. At the solstice an intense Hadley cell has extended across the equator with maximum ascending motion taking place over land near 20°N, which is close to the region of maximum solar heating. Equally strong descending motion is apparent in the winter subtropics and low latitudes. The summer hemisphere reverse cell in mid-latitudes

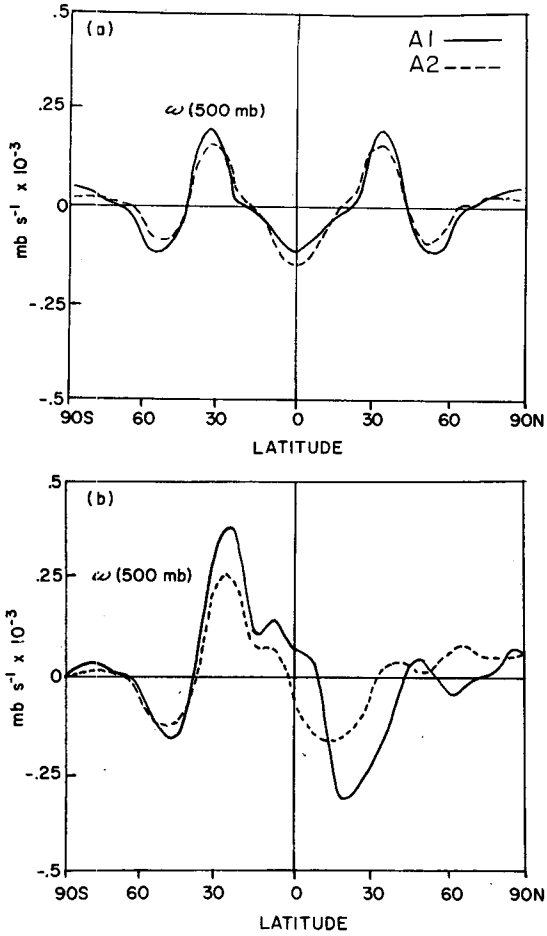


FIG. 15. As in Fig. 13 except for the vertical velocity field at 500 mb.

has disappeared although it is somewhat stronger and more equatorward in the winter hemisphere than at the equinox. The Hadley cell over the ocean is weaker by almost a factor of 2 and more equatorward than its counterpart in the A1 domain by about 10° of latitude. Corresponding to this displacement, the region of maximum ascending motion is nearer to 14°N over the ocean.

The most marked difference between the two atmospheric domains at the equinox appears in the temperature structure shown in Fig. 16a. The different forms of lower boundary condition show up most clearly at the surface (1000 mb), where the land temperature is considerably warmer than the ocean in equatorial and subtropical regions. The maximum land temperature at the equator of 307 K is probably too warm but this would be reduced markedly if moist processes were taken into account. Moving toward the poles we note that the longitudinal temperature gradient reverses with the oceans becoming warmer than the continents by a small amount at middle to high latitudes. The small plateau on the oceanic surface temperature near 55°N corresponds to the convective adjustment regime of the ocean model. The poleward limit of the plateau is the sea-ice latitude which is predicted to be at 60°N and 60°S. Freezing latitudes over the land are somewhat equatorward at 55°N. The warmer sea-ice surface temperature is mainly a result of the heat flux through the ice ($F_I$) from the relatively warm ocean below. At the 250 mb level the temperature of the atmosphere over the land is warmer than that over the ocean at all latitudes. Over the land the strong subsidence shown in Fig. 15a in the subtropics is sufficient to produce relative maxima in the temperature distribution. Such features of the mean temperature structures along meridians passing through Africa and southern Europe have been commented on by Newell *et al.* (1972) and others.

The solstice temperature structures are shown in Fig. 16b and indicate maximum temperature near 30°N

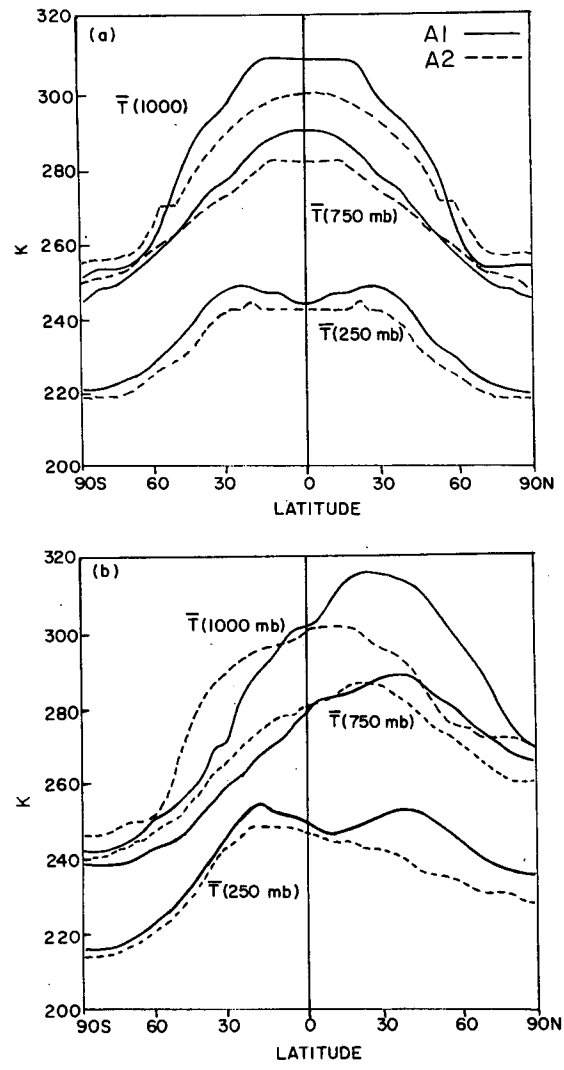


FIG. 16. As in Fig. 13 except for the 1000 mb (surface), 750 mb and the 250 mb temperatures.

over the land and 15°N over the ocean. Once again the surface temperatures are unrealistically high over the continent because of the omission of a hydrology cycle. In the winter hemisphere the east-west temperature gradient has reversed with the oceans being significantly warmer than the land. The sea-ice latitude is now near 50°S which is 10° poleward of the continental freezing latitude.

The ocean mixed layer depth is shown in Fig. 17. The stippled region denotes the sea-ice regime and the solid curve describes the mixed layer depth. The dashed line indicates the region where a finite mixed layer is not defined, i.e., the unstable and sea-ice regimes. Basically the distributions of $\bar{h}$ follow observation quite well (see, e.g., Alexander and Kim, 1976), with minima occurring at low and mid-latitudes during the equinox, separated by maxima located in the subtropics. At the solstice $\bar{h}$ is generally small in the summer hemisphere and deeper in the winter hemisphere which also appears to tally with observation. Overall, the $\bar{h}$ distribution of Fig. 17 and the temperature structure indicated in Fig. 16, together with the heat transportations described by Lau (1976), provide an adequate description of the system. The major problem appears to be the latitude of sea-ice formation which is too far equatorward in both experiments. This probably results from the extremely simple ice formation model utilized in this study.

## 6. Concluding remarks

The theory and results of a simple phenomenological model have been presented. The steering philosophy was to develop the simplest framework which could include atmospheric-oceanic interaction and an explicit representation of continentality. The model structure comprised of a series of pole-to-pole primitive equation atmospheres (although, in general, the domains may have arbitrary latitudinal and longitudinal extent as shown in Fig. 17) which are contained within and are averaged over finite longitudinal widths. Such atmospheres overlay and were coupled to either a simple ocean model, which in this case was a modified advective Kraus-Turner model, or to a continental region. A simple parameterization representing the interaction between adjacent atmospheric domains was developed.

The results of the experiment using the dry version of the model for both equinox and solstice conditions show that although the various domains respond to the radiational forcing in different manners, which reflect the different response time scale inherent in their basic physics, there is a strong interaction between the domains by the interdomain interaction terms. Such terms, which are generally smaller than the north-south eddy fluxes of heat and momentum, are still substantial and act as agents attempting to equalize the contrasts between the atmospheric domains over the ocean and atmosphere. Such a role is especially obvious in the

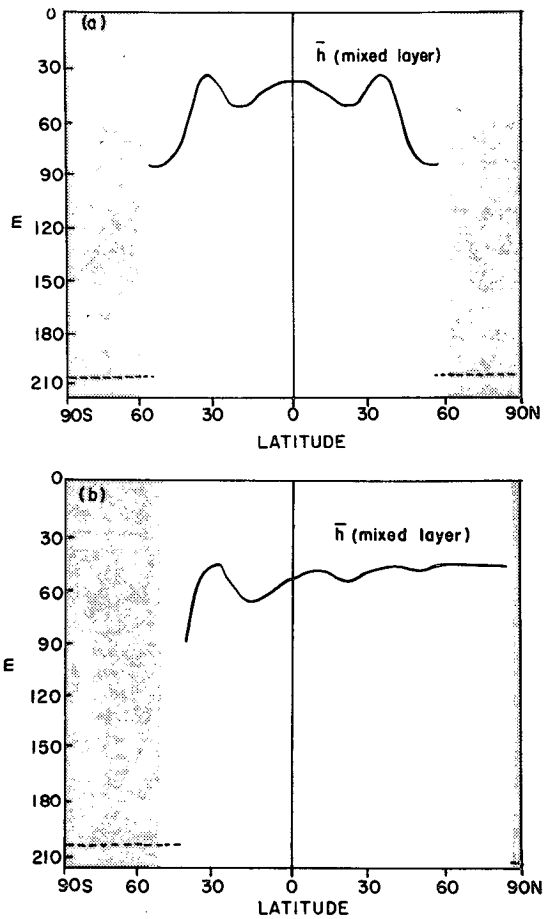


FIG. 17. Latitudinal distribution of mixed-layer depth $\bar{h}$ for (a) the equinox and (b) the solstice. Solid curve represents mixed layer depth in mixed layer regime. Dashed curve indicates absence of mixed-layer definition. Stippled area denotes sea ice regime.

Northern Hemisphere summer solstice case where, for example, the convergence of heat into the ocean domain has magnitudes of about 1.5 K day$^{-1}$ which compares to the north-south eddy heat flux convergence in the winter hemisphere of 2 K day$^{-1}$ and is longer than the 0.4 K day$^{-1}$ occurring in the north-south direction in the summer hemisphere. In the equinox case the north-south eddy fluxes are much larger than their inter-domain counterparts, but at this time the differences between the two domains are quite small. In the absence of collaborating data, the best that can be said is that the east-west or interdomain parameterizations are behaving as one might expect large-scale thermally driven quasi-stationary waves to behave in the real atmosphere, *viz.*, acting as longitudinal connections between differently forced regions and as regulators between these regions by the mutual, and at least partial, imposition upon each region of the basic time scales of the other domain.

A further experiment has been performed using the same model. Rather than seeking converged results, the

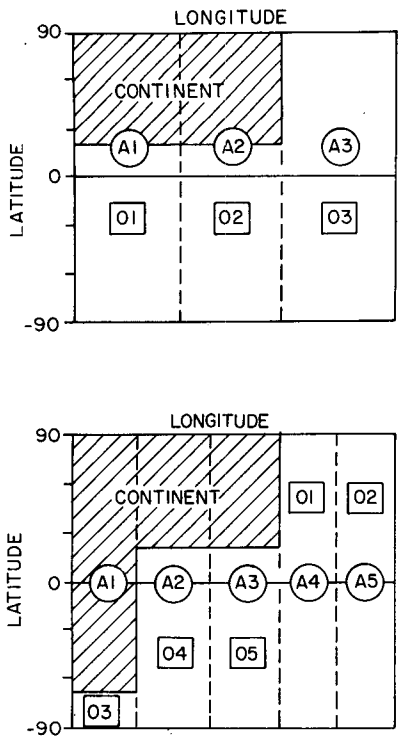


FIG. 18. Schematic representation of two proposed domain configurations for a monsoon experiment (upper) and an annual cycle experiment (lower).

experiment seeks the response of the model to *variable* solar heating which is followed through a complete annual cycle starting from the converged equinox state. The results differ from those described in the text with the summer solstice fields less intense than in the converged case. The results of the experiment are discussed by Lau and Webster (1977).

The obvious drawback that all models possess which reduce or simplify the total degrees of freedom (e.g., the zonally averaged or domain averaged model types) is that they require parameterizations to involve large-scale eddy processes. As the model results may be very sensitive to the parameterization scheme chosen or developed, it is important that the parameterizations are as representative as possible of real processes. Unfortunately, the parameterizations used possess some problems and point toward the development of some generalized parameterization which will allow treatment of both transient disturbances and stationary eddies.

In choosing the latitudinal eddy schemes it was pointed out in Section 3 that they all refer to growing baroclinic disturbances, the parameterization emerging from linear baroclinic instability theory. Implicit in the use of such schemes, then, is an assumption that the behavior of mature disturbances is well approximated by incipient eddies or that the majority of the heat and momentum is transported by the growing disturbances. Quite possibly, both assumptions are tenuous. In the first place, latitude-longitude fields of mean transient eddy flux (e.g., Newell *et al.*, 1972; Webster and Curtin, 1975; Blackmon *et al.*, 1977) show distinct longitudinal variations in eddy heat and momentum fluxes, with the maxima occurring downstream of the cyclogenesis regions. The relative positions of the formation and transportation maximum regions suggest that a large proportion of the total heat and momentum fluxes are accomplished by mature disturbances. Second, Blackmon *et al.* (1977) note that the storm tracks (i.e., the average trajectories of mature disturbances emanating from their formation regions) coincides with the strongest surface baroclinicity and not the strongest baroclinicity in the free atmosphere. Consequently, the distribution of eddy momentum flux relative to the jet stream by mature disturbances will differ considerably to the fluxes calculated by assuming growing disturbances because the strong baroclinic regions near the ground are considerably poleward of the free atmosphere maximum baroclinicity (Blackmon *et al.*, 1977). Quite possibly studies such as that by Blackmon *et al.* will lead to a better understanding of the role of eddy flux in the atmosphere and, possibly the development of more representative parameterizations. Furthermore it is hoped that the domain-averaged formulation will lend itself as an adequate framework upon which such a parameterization can be based.

The interdomain flux parameterization scheme developed in Section 3 represents a first attempt and in many respects is incomplete. This is because it deals mainly with zonal fluxes by large-scale and quasi-stationary eddies only, thus neglecting representation of any contribution in the zonal direction by the transient eddies. Such an assumption may be rather poor especially with the observed variability of transient eddies and storm tracks (Blackmon *et al.*, 1977). Unfortunately, the inclusion of such effects must await the development of a unified parameterization that will make use of the interdomain variability of the various main states.

The neglect of a hydrology cycle in the experiments discussed in this paper is done with the realization that it is an important and possibly dominant process in the atmosphere, especially at low latitudes. However, in the development of a relatively new type of model we prefer to consider the simplest system first. Whereas moist processes and the addition of clouds are of first priority, the inclusion of a wind-driven component to the ocean circulation is also under study.

Beyond the annual cycle experiment to be reported by Lau and Webster (1977), an experiment aimed at studying a monsoon sequence developed by a land-dominated hemisphere and by an oceanic hemisphere is planned. The domain configuration required to model such a system is shown in the upper diagram of Fig. 18 and consists of two atmospheric domains surmounting a pole-to-pole ocean domain and an ocean domain

truncated by a continental region. The lower diagram indicates a possible domain configuration to study details of the annual cycle.

## APPENDIX

## Numerics

The momentum and thermodynamic equations of (1) were expressed at 250 and 750 mb and the continuity equation at 500 mb in each domain. Parameterizations were expressed at 250 and 750 mb except for the vertical fluxes which are represented at 500 mb. Time differencing was accomplished by use of the time-smoothed version of the leapfrog scheme with the filter

$$\bar{f}(t)=f(t)+\tfrac{1}{2}\nu[\overline{f(t-\Delta t)}-2f(t)+f(t+\Delta t)]$$

which has been analyzed by Asselin (1972). The response of the filter $\bar{X}$ is

$$\bar{X}=\frac{(2-\nu)^2+2\nu^2(1-\cos\omega\Delta t)\exp(i\omega t)}{(2-\nu)^2+4\nu(1-\cos\omega\Delta t)}$$

which for different values of $\nu$ provides strong damping in the high-frequency waves while leaving low frequencies relatively unaffected. It also has the additional advantage of having no negative response for waves with periods $<2\Delta t$, as distinct from the conventional 1-2-1 filter. Used in conjunction with the leapfrog scheme, the filter very quickly removes both the computational mode and the high-frequency waves. In our model we choose $\nu=1$ so that $\omega\Delta t<0.57$. The damping is strongest for $\omega\Delta t=0.5$ [see Asselin (1972) for details].

In the actual time-marching process, we start with the domain-averaged fields $\bar{u}_{l,k}$, $\bar{v}_{l,k}$, $\bar{T}_{l,k}$, etc., at time steps $N$ and $N+1$; $l$ and $k$ denote latitude and pressure grid points, respectively. Using the thermodynamic equation of (1) in finite-difference form, $\bar{T}_{l,k}^{N+1}$ is calculated which allows the calculation of $\bar{\psi}_{l,k}^{N+1}$. Knowledge of $\bar{\psi}_{l,k}^{N+1}$ renders the momentum equations to a set of coupled quations in $\bar{u}_{l,k}^{N+1}$, $\bar{v}_{l,k}^{N+1}$, $\bar{u}_{l,k}^{N+1}$, etc., with the form

$$\bar{u}_{l,k}^{N+1}=\bar{u}_{l,k}^{N-1}+2\Delta t[(\text{advection})^N+(\text{diffusion})^{N-1}+(f_l+a^{-1}\tan\phi_l\bar{u}_{l,k}^N)(\bar{v}_{l,k}^{N+1}+\bar{v}_{l,k}^{N-1})/2],$$

$$\bar{v}_{l,k}^{N+1}=\bar{v}_{l,k}^{N-1}+2\Delta t[(\text{advection})^N+(\text{diffusion})^{N-1}-(a^{-1}\partial\bar{\psi}/\partial\phi)_{l,k}^{N+1}-(f_l+a^{-1}\tan\phi_l\bar{u}_{l,k}^N)\times(\bar{u}_{l,k}^{N+1}+\bar{u}_{l,k}^{N-1})/2],$$

which may be solved by Cramer's rule. With $\bar{T}$, $\bar{\psi}$, $\bar{u}$ and $\bar{v}$ at $N+1$, $\bar{\omega}^{N+1}$ is obtained from continuity.

In the initial stages of computation the $\bar{v}$ field is rather noisy due to the presence of the two-grid wave. In order to reduce this a 1-2-1 spatial filter was applied at every time step. After a number of days of simulated time, the frequency of spatial smoothing was reduced to once every 24 time steps.

The maximum time step at which the centered space difference and quasi-semi-implicit filtered time-difference scheme can handle and still remain stable is 1 h 20 min for the atmosphere. The computation time for a two atmospheric domain-averaged model with an interactive coean mixed layer is roughly 1.2 h per simulated year on a CDC 6400.

*Acknowledgment.* This work was supported by the Atmospheric Sciences Section, National Science Foundation, under Grant DES-74-01762.

## REFERENCES

Alexander, R. C., and J. W. Kim, 1976: Diagnostic model study of mixed layer depths in the summer North Pacific. *J. Phys. Oceanogr.*, **6**, 293–298.

Arakawa, A., A. Katayama and Y. Mintz, 1968: Numerical simulation of the general circulation of the atmosphere. *Proc. WMO-IUGG Symp. Numerical Weather Prediction*, Japan Meteor. Agency, IV-7b to IV-8b.

Asselin, R., 1972: Frequency filter for time integration. *Mon. Wea. Rev.* **100**, 487–490.

Bates, J. R., 1970: Dynamics of disturbances on the intertropical convergence zone. *Quart. J. Roy. Meteor. Soc.*, **96**, 677–701.

Bjerknes, J., 1969: Atmospheric teleconnections from the equatorial Pacific. *Mon. Wea. Rev.*, **97**, 163–172.

Blackmon, M. L., J. M. Wallace, N.-C. Lau and S. L. Mullen, 1977: An observational study of the northern hemisphere wintertime circulation. *J. Atmos. Sci.*, **34**, 1040–1053.

Bryan, K., S. Manabe and R. C. Pacanowski, 1975: A global ocean atmosphere model. Part II. The oceanic circulation. *J. Phys. Oceanogr.*, **5**, 30–46.

Budyko, M. I., 1969: The effect of solar radiation variations on the climate of the earth. *Tellus*, **21**, 61–69.

Charney, J., 1959: On the general circulation of the atmosphere. *The Atmosphere and the Sea in Motion*, Rockefeller Institute Press, 178–193.

Denman, K. L., 1973: A time-dependent model of the upper ocean. *J. Phys. Oceanogr.*, **3**, 173–184.

Faegre, A., 1972: An intransitive model of the earth-atmosphere-ocean system. *J. Appl. Meteor.*, **11**, 4–6.

Green, J. S. A., 1970: Transfer properties of the large scale eddies and the general circulation of the atmosphere. *Quart. J. Roy. Meteor. Soc.*, **96**, 157–185.

Hayashi, Y., 1974: Spectral analysis of tropical disturbances appearing in a GFDL general circulation model. *J. Atmos. Sci.*, **31**, 180–218.

Holloway, J. L., Jr., and S. Manabe, 1971: Simulation of climate by a general circulation model. I. Hydrology cycle and heat balance. *Mon. Wea. Rev.*, **99**, 335–369.

Holton, J. R., and D. Colton, 1972: A diagnostic study of the vorticity balance at 200 mb in the tropics in the northern summer. *J. Atmos. Sci.*, **29**, 1124–1128.

Hunt, B. G., 1973: Zonally symmetric global general circulation models with and without the hydrology cycle. *Tellus*, **15**, 337–354.

Kato, H., and O. M. Phillips, 1969: On the penetration of a turbulent layer into a stratified fluid. *J. Fluid Mech.*, **37**, 643–655.

Kraus, E. B., and J. A. Turner, 1967: A one-dimensional model of the seasonal thermocline: II. The general theory and its consequences. *Tellus*, **19**, 98–105.

Krishnamurti, T. N., 1971: Tropical east-west circulations during the northern summer. *J. Atmos. Sci.*, **28**, 1324–1347.

Lahiff, L. N., 1975: A low-latitude atmosphere-ocean climate model. *J. Atmos. Sci.*, **32**, 657–674.

Lau, K. M. W., 1977: A simple advective global mixed-layer model. Submitted to *J. Phys. Oceanogr.*

——, and P. J. Webster, 1977: Simulation of the annual cycle with a simple interactive ocean-atmosphere model. To be submitted to *J. Atmos. Sci.*

Leetmaa, A., 1972: The response of the Somali-current to the Southwest monsoon of 1970. *Deep Sea Res.*, **19**, 319–325.

McCracken, M. C., 1973: Zonal atmospheric model ZAM2. *Proc. Second Conf. Climatic Impact Assessment Program*, U.S. Dept. of Transportation, Rep. DOT-TSC-OST-73-4, Boston, 298–320.

Manabe, S., and T. B. Terpstra, 1974: The effects of mountains on the general circulation of the atmosphere as identified by numerical experiments. *J. Atmos. Sci.*, **31**, 3–42.

——, J. Smagorinsky and R. F. Strickler, 1965: Simulated climatology of a general circulation model with a hydrology cycle. *Mon. Wea. Rev.*, **93**, 769–798.

——, K. Bryan and M. J. Spelman, 1975: A global ocean-atmospheric climate model. Part I. The atmospheric circulation. *J. Phys. Oceanogr.*, **5**, 3–29.

Namias, J., 1971: The 1968–69 winter as an outgrowth of sea and air coupling during antecedent seasons. *J. Phys. Oceanogr.*, **1**, 68–81.

——, 1972: Experiments in objectively predicting some atmospheric and oceanic variables for the winter of 1971–72. *J. Appl. Meteor.*, **11**, 1104–1174.

——, 1976: Some statistical and synoptic characteristics associated with El Niño. *J. Phys. Oceanogr.*, **6**, 130–138.

Newell, R. E., J. W. Kidson, D. G. Vincent and G. J. Boer, 1972: *The General Circulation of the Tropical Atmosphere and Interactions with Extratropical Latitudes*, Vol. 1, The MIT Press, 258 pp.

North, G. R., 1975a: Analytic solution to a simple climate model with diffusive heat transport. *J. Atmos. Sci.*, **31**, 1301–1307.

——, 1975b: Theory of energy-balance climate models. *J. Atmos. Sci.*, **31**, 2033–2043.

Oort, A. H., and E. M. Rasmusson, 1971: Atmospheric circulation statistics. NOAA, Prof. Pap. No. 5, U.S. Dept. of Commerce. 323 pp.

Palmén, E., and C. W. Newton, 1969: *Atmospheric Circulation Systems: Their Structure and Physical Interpretations*. Academic Press, 603 pp.

Pike, A. C., 1971: Intertropical convergence zone studied with an interacting atmosphere and ocean model. *Mon. Wea. Rev.*, **99**, 469–477.

Pyke, C. B., 1965: On the role of air-sea interaction in the development of cyclones. *Bull. Amer. Meteor. Soc.*, **46**, 4–15.

Ramage, C. S., 1975: Preliminary discussion of the meteorology of the 1972–73 El Niño. *Bull. Amer. Meteor. Soc.*, **56**, 234–242.

Saltzman, B., and A. D. Vernekar, 1971: An equilibrium solution of the axially symmetric component of the earth's macroclimate. *J. Geophys. Res.*, **76**, 1498–1524.

Schneider, S. H., and T. Gal-Chen, 1973: Numerical experiments in climate stability. *J. Geophys. Res.*, **78**, 6182–6194.

Sellers, W. D., 1969: A global climate model based on the energy balance of the earth-atmosphere system. *J. Appl. Meteor.*, **8**, 392–400.

Shukla, J., 1975: Effect of the Arabian Sea surface temperature anomaly on Indian summer monsoon: a numerical experiment with the GFDL model. *J. Atmos. Sci.*, **32**, 503–511.

Smagorinsky, J., 1953: The dynamical influence of large-scale heat sources and sinks on the quasi-stationary mean motion of the atmosphere. *Quart. J. Roy. Meteor. Soc.*, **97**, 342–366.

Stone, P. H., 1973: The effect of large scale eddies on climate change. *J. Atmos. Sci.*, **30**, 521–529.

——, 1974: The meridional variation of the eddy fluxes by baroclinic waves and their parameterization. *J. Atmos. Sci.*, **31**, 444–456.

Trenberth, K., 1976: Fluctuations and trends in indices of the Southern Hemispheric circulation. *Quart. J. Roy. Meteor. Soc.*, **102**, 65–76.

Turner, J. S., and Kraus, E. B., 1967: A one-dimensional model of the seasonal thermocline, I, A laboratory experiment and its interpretation. *Tellus*, **19**, 88–97.

Washington, W. M., and A. Kasahara, 1970: A January simulation experiment with the two-layer version of the NCAR global circulation model. *Mon. Wea. Rev.*, **98**, 559–580.

Webster, P. J., 1973: Temporal variation of low-latitude zonal circulations. *Mon. Wea. Rev.*, **101**, 803–816.

——, and D. G. Curtin, 1975: Interpretations of the EOLE experiment. II, Spatial variation of transient and stationary modes. *J. Atmos. Sci.*, **32**, 1848–1863.

Wiin-Nielson, A., and J. Sela, 1971: On the transport of quasi-geostrophic vorticity. *Mon. Wea. Rev.*, **99**, 447–459.

Wyrtki, K., 1961: The thermohaline circulation in relation to the general circulation in the oceans. *Deep Sea Res.*, **8**, 39–64.